ORIGINAL ARTICLE

Investigating structural diversity in selected antioxidants – A virtual and experimental approach

Janhvi Dureja, Renu Chadha*, Maninder Karan, Akshita Jindal, Kunal Chadha

Dureja J, Chadha R, Karan M, et al. Investigating structural diversity in selected antioxidants – A virtual and experimental approach. J Pharm Chem Pharmacol. 2018;2(1):11-37.

BACKGROUND: The present manuscript highlights the material pursuits of selected antioxidants i.e., gentisic acid and L-tyrosine by exploring their various polymorphic modifications using virtual and experimental approach.

METHODS: Polymorph Prediction/Crystal structure prediction (CSP) was undertaken using Polymorph Predictor module of BIOVIA Material Studio software. The lattice energy landscape representing various low energy and high density polymorphic forms was generated. Simultaneously various solid forms were experimentally isolated from different solvents/or solvent mixtures. Their characterization using various analytical tools was done. Crystal structure determination was carried out using Reflux Plus module of BIOVIA Material Studio software. Lattice energy landscape was scanned to hunt for these observed forms. Crystal morphology study was performed to ascertain morphologically important (M.I.) facets. The solubility behavior and intrinsic dissolution rate of these forms were then determined to evaluate their behavior in solution form. Besides this, *in vivo* (animal) studies based on the behavioral patterns were performed to check their clinical relevance.

RESULTS: Four polymorphs (including the form present in commercial sample), one solvatomorph of gentisic acid, three forms of L-tyrosine (including the form present in commercial sample), and one solvatomorph of L-tyrosine were obtained from various solvents/or solvent mixtures. It was noticed that these experimentally isolated forms were present as local minima in the lattice energy landscape of predicted structures of the respective drug molecules. It was observed that form III each of gentisic acid and L-tyrosine was found out to be most soluble amongst other forms of these antioxidants. The animal studies reflecting behavioral changes further supported the clinical effectiveness of form II and III of gentisic acid and form III of L-tyrosine.

CONCLUSION: This research work illustrates the relevance of CSP in studying the various polymorphic modifications of chosen drug moieties. Crystal structure determination from PXRD patterns is a reliable approach towards drug development process. The information generated from various material findings, *in vitro* and *in vivo* studies of selected antioxidants can be useful in the emerging field of anti-ageing therapy.

Key Words: *Gentisic acid; L-tyrosine; Powder X- ray diffraction (PXRD) pattern; Crystal structure prediction (CSP); Lattice energy landscape; Crystal morphology; Behavioral patterns.*

INTRODUCTION

Polymorphism is the tendency of a chemical to exist in various structural forms. Polymorphism has become even more relevant in chemical and food industry as it has contributed significant variability in product performance and continues to pose a challenge to pharmaceutical scientists in producing drugs of consistent quality [1,2]. Solvatomorphism is used to express crystal variations of the substance where the unit cells differ in their elemental composition through the inclusion of one or more solvent molecules [3-7]. These solid forms of drug molecules differ in their physico-chemical attributes like dissolution, solubility, physical stability, flowability and hygroscopicity. The outcome is variable bioavailability, drug efficacy and even toxicity [8,9]. Thus it is quite necessary to have an in-depth knowledge of these forms in order to generate a quality drug molecule. The present work has unveiled the concept of polymorphism in two antioxidant molecules, L-tyrosine and gentisic acid. Superintending the ageing process is always a choicest matter of discussions. Ageing is an unstoppable process, yet some control can be exercised over it [10,11]. The free radicals generated over time as a result of aerobic metabolism in organisms get accumulated in cells and cause oxidative damage to cells and tissues. This can be the root cause of various age-related ailments such as atherosclerosis, Parkinsonism, diabetes, cancer, asthma, cataracts and senile dementia. On the basis of free radical theory of ageing, it is postulated that any substance with antioxidant capacity can be a useful candidate for delaying the ageing [12]. L-tyrosine and gentisic acid are the potential candidates with antioxidant capacity [13-16]. To better understand their anti-ageing activity, development and research on these functional foods is of utmost interest to both public and scientific community. The literature reports show that these dietary supplements exhibit poor water solubility and hence bioavailability [8] and also their material aspects are not much explored. Thus present work has undertaken improvement of their physicochemical and biopharmaceutical parameters following crystal tailoring approach by predicting and preparing their various polymorphs and solvatomorphs [1-3,8,12-22].

Literature report highlights only two polymorphic forms of gentisic acid [23-25] and one of L-tyrosine [26,27] and there is no information available on solvatomorphism in these molecular entities. Moreover, there is no data available on crystal morphology and habit properties of chosen antioxidant molecules. The present work highlights the virtual approach towards detection of polymorphic tendency of chosen drugs through crystal structure prediction (CSP). This is further utilized to hunt the experimentally observed crystal forms in the lattice energy landscape generated from predicted structures. All the observed forms tend to lie as local minima in these predicted structures within lower energy regions in crystal energy landscape (approx. 7 kcal/mole). The comparison of lattice parameters of predicted polymorphs with observed crystal structures is done in order to check the reliability of CSP using Biovia Material Studio (MS). Thus the study highly recommends that polymorph prediction [28,29] should be done prior to experimental screening which is quite expensive, tedious and time- consuming. Selection of polymorph with optimum properties is a prerequisite in formulation and development for crystalline products [1,8,22]. The predicted polymorphs show different packing arrangement, which subsequently give a choice to prepare and modify a crystal form with desired physico-chemical properties. The study also assists in understanding of crystal structure by interpreting the intermolecular forces involved in crystals without much work involved in their preparation [30]. Furthermore, the effect of crystal habit and in turn crystal morphology on the polymorphic features particular drug do also need attention. Crystal morphology is a key parameter to examine the quality attributes of a crystalline material such as tablet compressibility, mechanical strength and powder flowability [31-33]. This in turn has a great impact on bioavailability and therapeutic response of a particular drug. Thus sound knowledge of crystal morphology and crystal habit is must in designing a more favorable dosage form. Computational screening of all the plausible low energy polymorphs and the knowledge of their crystal habit will enhance the quality and speed of designing a drug molecule with

University Institute of Pharmaceutical Sciences (UIPS), Panjab University, Chandigarh, India.

Correspondence: Dr. Renu Chadha Ph.D, (University Institute of Pharmaceutical Sciences UIPS), Panjab University, Chandigarh, India. Telephone: + 08037198460, e-mail: renukchadha@rediffmail.com

Received: September 20, 2018, Accepted: November 27, 2018, Published: December 04, 2018

desirable characteristics and thus improving the efficiency of R&D [34,35]. The other important arena of research is to evaluate the potential of powder X-ray diffraction (PXRD) patterns in crystal structure determination using MS [36-38] and to check its reliability in the chosen drug molecules. The present study deals with the prediction of various polymorphic forms/or solvatomorphs of gentisic acid and L-tyrosine followed by their preparation and characterization using melting point determination, differential scanning calorimetry (DSC), fourier transform infrared (FTIR) spectroscopy and powder X-ray diffraction (PXRD) method. The experimentally prepared polymorphs were also evaluated for their physicochemical properties like solubility, intrinsic dissolution rate (IDR) and enthalpy of solution. The newly generated solid forms were then subjected to *in vivo* studies in order to establish their clinical efficacy.

METHODS

Prediction of polymorphs/Solvatomorphs

Polymorph module of Biovia Material Studio (MS) software suite, version 7.0 [39] was employed to predict the possible polymorphs and solvatomorphs of selected drug molecules. The initial geometry optimization with Dmol3 using COMPASS forcefield, an in-built energy minimization strategy of MS, generates an input structure for polymorph screening. The polymorh search was repeated thrice within most common space groups of interest i.e. P-1, P21/c, P212121, Pbca, C2/c, P21 and P2/c [40] until convergence of all generated crystal structures to equal energy minima. It involves packing step (packing in a unit cell) which uses Monte Carlo simulation, followed by pre-clustering, optimization and then clustering. The generated plausible crystal structures falling in specific space groups were further interpreted by plotting energy versus density plot i.e. crystal lattice energy landscape in order to hunt the local minima, global minima and thermodynamically stable form.

Experimental screening

The commercial samples of L-tyrosine and gentisic acid were procured from from Alfa Aesar (Thermo Fisher Scientific). Different polymorphs and solvatomorphs of gentisic acid and L-tyrosine were successfully generated by slow evaporation and anti-solvent techniques using various solvents/ or solvent mixture (Table 1). Crystals appeared in a month were further subjected to characterization.

Characterization of crystal forms

Determination of melting point

The melting points of all the forms of selected drugs were determined on a digital melting point apparatus.

Differential scanning calorimetry (DSC)

The DSC thermograms were obtained using Q20 DSC instrument. The sample (2-5 mg) was placed into sealed aluminium pans and scanned (50-300°C) at a rate of 10°C/min under nitrogen purge of 50 mL/min. TA Q series advantage software (Universal analysis 2000, software) was used for data management.

TABLE 1

Solvent/solvent systems used to successfully isolate different forms of selected drugs

Solvents	Crystal form
Gentisic acid	
Aqueous Ethanol	BESKAL 02*
Aq. Ethanol+ Chloroform + Acetone	BESKAL 03**
Ethanol + Acetone	Form I
Toluene+ Isopropanol	Form II
Methylene Chloride+ Ethanol	Form III
Formic Acid	Form IV (formic acid solvate; 1:1)
L- tyrosine	
Lactic acid+ water (1:2) + methanol (antisolvent)	Form I
Water+ lactic acid (2:1)	Form II
Water+ lactic acid (2:1)+ Tetrahydrofuran (antisolvent)	Form III
Lactic acid+ water (2:1) + acetonitrile (antisolvent)	Form IV (acetonitrile solvate; 1:1)

Thermogravimetric analysis (TGA)

TGA scans of the solvates (1- 10 mg) of selected drug molecules were obtained on TGA instrument using aluminium pan at a heating rate of 10 °C/min. under nitrogen purge of 50 ml/min. The weight loss percent (of solvent) was accounted based on the mass of the original sample.

Powder X- Ray Diffraction (PXRD)

The diffractograms of all the observed forms were recorded on X'PERT-PRO diffractometer using Cu- Kα radiation (1.54 A°). The Cu anode tube voltage and current were adjusted to 45 kV and 40 mA respectively. The slit size was set to 0.48°. The sample (about 200 mg) was then loaded and scanned at 2θ values ranging from 3.5° to 49° with a step size of 0.0170° and scan step time set to 25.1996 s. The PXRD patterns were analyzed using X'PERT high score software.

Fourier transform infra-red spectroscopy (FTIR) spectroscopy

The FTIR spectra of observed crystal forms were obtained using Perkin-Elmer RX-1 FTIR spectrophotometer (UK). Drug sample (2- 4 mg) was dispersed in finely ground KBr (approx. 20 mg), triturated in agate pestle mortar and then pressed in a manual press to form a pellet. The spectral data was collected over the range of 450- 4000 cm^{-1}.

Optical microscopy

To study the overall macroscopic crystal habit of the different polymorphs, optical micrographs of all the samples were taken using a Leica DM3000 upright optical microscope with polarizer setting. The images were taken at resolution of 25x.

Crystal structure determination

The PXRD patterns of observed forms of drug molecules were subjected to Reflex Plus module of Material Studio. The crystal structure determination was carried out following four basic steps i.e. indexing, Pawley fitting/ refinement, structure solution and Rietveld refinement [40].

The peaks were indexed using X-cell (Newmann, 2003) indexing program to obtain various solutions of crystal lattices. The unit cell with highest figure of merit (FOM) was selected and was further subjected to Pawley fitting/ refinement to get the accurate lattice constants and lattice parameters. The unit cell was optimized from 10 cycles and space groups were searched. The optimized structure of drug molecule was imported into the refined empty unit cell and it was subjected to Powder Solve programof Reflex Plus module of MS for structure solution [40,41]. The similarity R_{wp} between a simulated and an experimental diffraction pattern was confirmed by the R_{wp} (weighted Rietveld parameter) values obtained after Rietveld refinement. The final structure solution was then optimized using Forcite module of MS.

Morphology prediction

The morphology simulation of the observed polymorphic modifications of both the antioxidant molecules was done using the Morphology module MS [42,43]. The minimum inter- planar spacing (d_{hkl}) for face list generation was set to 1.0 A° and the maximum absolute values for the Miller indices h, k, and l for the faces were set to 5, 5, and 5 respectively with an upper limit of 100 growing faces. Growth morphology algorithm generates growth faces along with their attachment energy (E_{att}). The algorithm is based on the hypothesis that crystal face growth rate is proportional to its attachment energy [42-46].

Solubility study

The solubility studies of various forms of selected drugs were performed by shaking an excess of drug (approx. 20 mg) in 10 ml of distilled water using MSW-275 (Macro scientific works, New Delhi) water bath shaker at 37°C for 24 hrs at 200 rpm. The aliquots were filtered through 0.45 µm membrane filter and analyzed spectrophotometrically at λ_{max} = at 325 nm, $E^{1\%}_{1\ cm}$ = 3,426 for gentisic acid and λ_{max} = 270 nm, $E^{1\%}_{1\ cm}$ = 239 for L-tyrosine.

Concentration of various forms was calculated using the formula:

$$\text{Concentration} = \frac{\text{Absorbance} \times \text{Dilution factor}}{E^{1\%}_{1\ cm}}$$

Intrinsic dissolution rate determination

The dissolution studies of polymorphic modifications of selected drug molecules were carried using rotating disc dissolution test apparatus DS 8000 in 900 mL phosphate buffer 7.4 with 100 rpm at 37°C for 1 hr.

The pellet of sample (100 mg) was formed with the help of die and punch and then compressed by tablet press. The die with pellet was mounted on dissolution apparatus holder and immersed in dissolution media. An aliquot of 5 ml was collected at 5, 10, 15, 20, 30, 40, 50 and 60 min and replenished with fresh dissolution medium. The samples were filtered through a 0.45 µm membrane filter and analyzed spectrophotometrically at their respective λ_{max} as mentioned under solubility studies. All experiments were carried out in triplicate.

In vivo **studies**

The study approved by the Institutional Animal Ethics Committee (IAEC/411, 11/9/2013) and Committee for Control and Supervision of Experimentation on Animals (CPCSEAs), Government of India was performed on adult male wistar rats (200–270 g, 17-18 months old). Animals were acclimatized to laboratory conditions prior to experimentation at room temperature and were kept on standard pellet diet and water ad libitum. D-galactose was used to induce ageing in the animals [47]. All the experiments were carried out between 09:00 and 17:00 h.

D-galactose, commercial drug samples and suitable forms of chosen drugs i.e. forms II and III of gentisic acid and L-tyrosine were suspended in 0.5% w/v sodium-carboxy-methyl-cellulose (Na-CMC). Only few forms (selected on basis of their solubility and dissolution characteristics as determined above) were taken for animal studies as other forms could not be prepared in sufficient quantities. The animals randomly divided on the basis of their body weights into several groups (n = 6 animals in each group) were treated orally for 21 days as follows (Tables 2 and 3). Study of behavioral patterns was done based on Morris maze test and locomotor activity

Morris water maze task

Individual animals were tested in a spatial version of the Morris water maze (MWM) test [40,48-50]. The apparatus consisted of a circular water tank (150 cm diameter, 40 cm high, filled to a depth of 30 cm with water at 28 ± 1°C). A platform (4.5 cm diameter) was placed in one quadrant of the pool, 1cm above and below the water level during the acquisition and retention phase respectively. The tank was located in a large room where there were several brightly colored clues external to the maze; these were visible from the pool and could be used by the rats for spatial orientation. During each trial, the position of the clues remained unchanged throughout the study and animal was subjected to four consecutive trials with a gap of 5 min. The animal, gently placed in the water of the pool between quadrants, facing the wall of the pool (which was changed with each trial) was allowed to locate the platform. Then, animals were guided to remain on the platform for 20s. If animal failed to reach the platform within 90 s, the same was guided to reach the platform and remained there for next 5 s.

Acquisition phase training was provided to animals daily four consecutive training sessions from day 17 to 20. Each rat was put into the water in any one of four starting positions and time latency to reach the visual platform for escaping from water known as initial acquisition latency (IAL) also known as escape latency time (ELT) was measured.

Retention phase trial was performed after 24 h, i.e., on day 21 after IAL. The animal released randomly at one of the edges facing the wall of the pool was examined for memory retention or retrieval. The time spent in target quadrant (TSTQ) by animal on day 21 of the protocol was recorded as an index of working memory.

Locomotor Activity/Closed Field Activity

Digital actophotometer was used to assess the locomotor activity. Each animal was placed in a square (30 cm) closed arena equipped with infra-red light sensitive photocells (and values expressed as counts per 5 min [51].

Statistical analysis was performed using graph pad prism (Graph Pad Software, San Diego, CA, USA) method. Two-way analysis of variance (ANOVA) was used to assess the behavioral data and one-way ANOVA was utilized to analyze the retention. Post hoc comparisons between groups were made using Tukey's test. The $p<0.05$ was considered significant.

RESULTS

Crystal structure prediction (CSP)

The Polymorph predictor modules of Biovia Material Studio have done all the calculations assuming it as a blind test; no information of the experimental crystal structure was used a priori in our calculations. The only input of the CSP study of chosen drugs was their respective molecular structure (Figure 1); the primary result of the study is a list of possible crystal structures ranked on the basis of the calculated lattice energy at 0K.

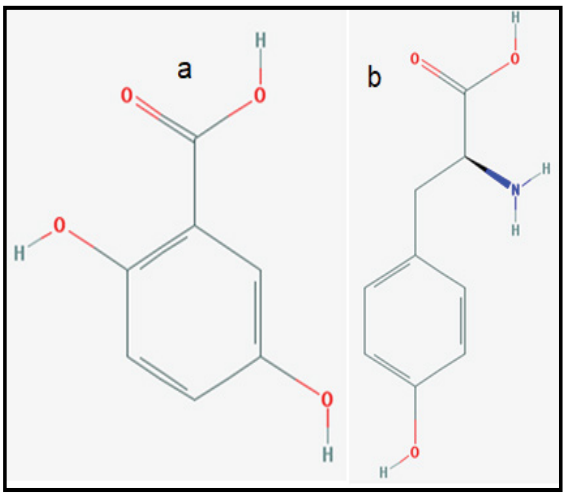

Figure 1) *Chemical structure of Gentisic acid (a) and L-tyrosine (b)*

Table 2

Treatment schedule I (Gentisic acid)

S. no.	Group name	Treatment
1	Naïve (untreated control)	0.5% sodium carboxymethyl cellulose (vehicle) (1 ml/kg)
2	Treated Control	D-galactose (100 mg/kg/day) (A)
3	G_a (BESKAL 02)	Commercial gentisic acid (25 mg/kg/day) + A
4	G_b (BESKAL 02)	Commercial gentisic acid (50 mg/kg/day) + A
5	II_a	Form I (25 mg/kg/day) + A
6	II_b	Form I (50 mg/kg/day) + A
7	III_a	Form II (25 mg/kg/day) + A
8	III_b	Form II (50 mg/kg/day) + A

TABLE 3

Treatment schedule II (L-tyrosine)

S. no.	Group name	Treatment
1	Naïve (untreated control)	0.5% sodium carboxymethyl cellulose (vehicle) (1 ml/kg)
2	Control	Treated D-galactose (100 mg/kg/day) (A)
3	Ia	Commercial tyrosine (500 mg/kg/day) + A
4	Ib	Commercial tyrosine (1000 mg/kg/day) + A
5	IIa	Form I (500 mg/kg/day) + A
6	IIb	Form I (1000 mg/kg/day) + A
7	IIIa	Form II (500 mg/kg/day) + A
8	IIIb	Form II (1000 mg/kg/day) + A

Out of the various predicted structures, 50 unique structures of gentisic acid (Table 4 and Figure 2), and 15 of L-tyrosine (Table 5, Figure 3) were selected. These correspond to structures with low energy and high density. These were further used to compare the crystal structures observed experimentally by finding out their location in their respective energy landscape diagrams (Figures 3 and 4).

Characterization

All the observed forms of chosen drugs were systematically characterized by thermoanalytical techniques (melting point, DSC and TGA), FTIR spectroscopy, PXRD and optical microscopy.

Thermal methods of analysis

Melting point

All forms of both drugs had shown variation in melting point (Table 6 and 7) from the commercial drug samples and from each other respectively suggesting the formation of new solid phases.

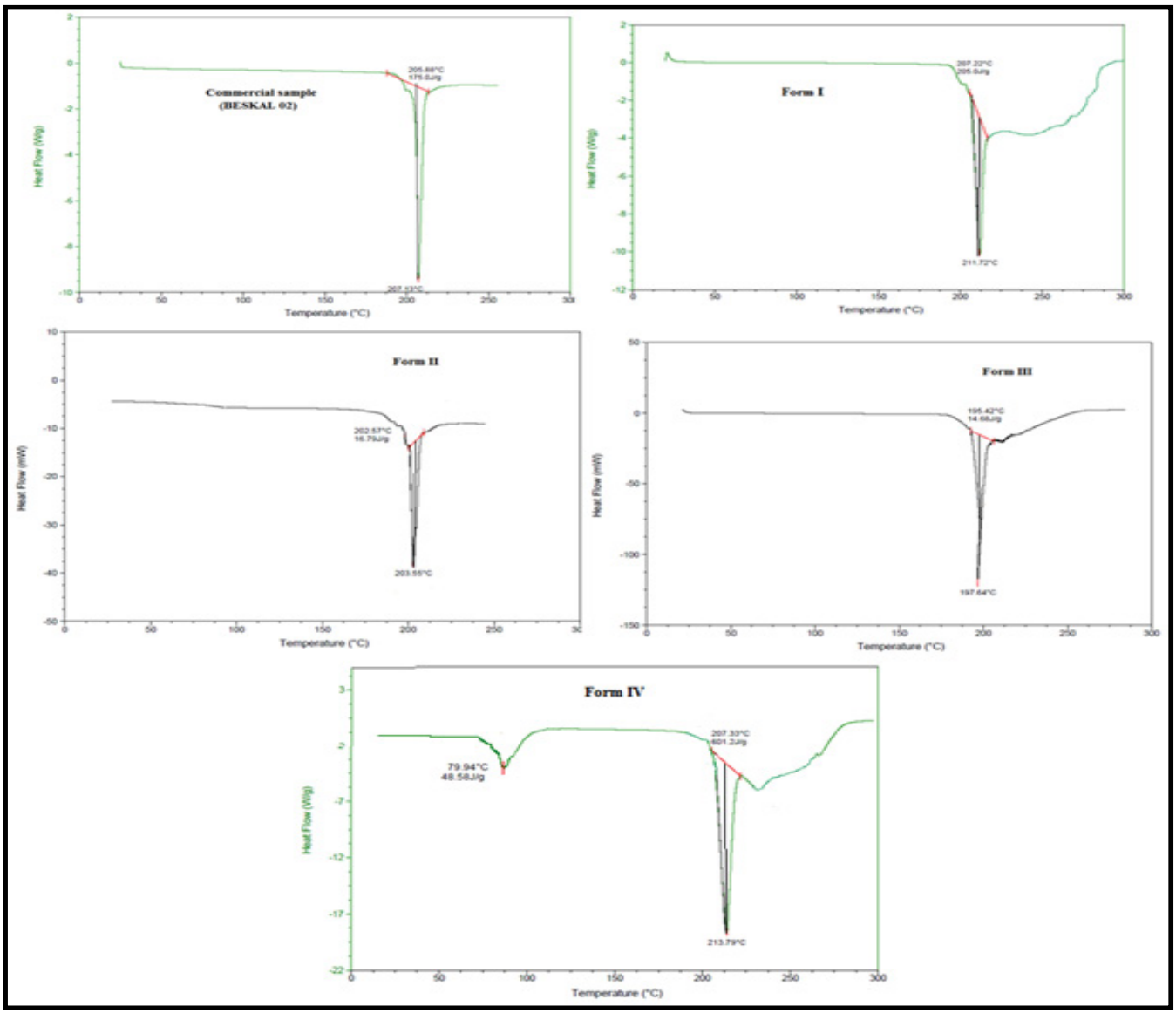

Figure 2) *DSC endotherms of various forms of gentisic acid*

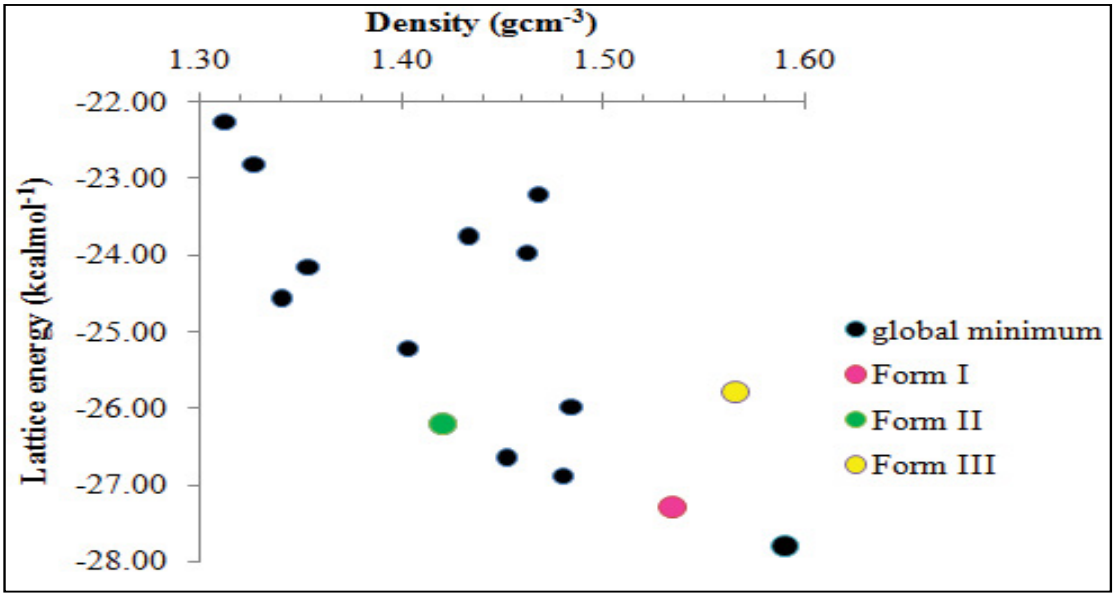

Figure 3) *Lattice energy landscape showing low energy and high density region encompassing experimentally observed three crystal forms of L-tyrosine generated through CSP runs*

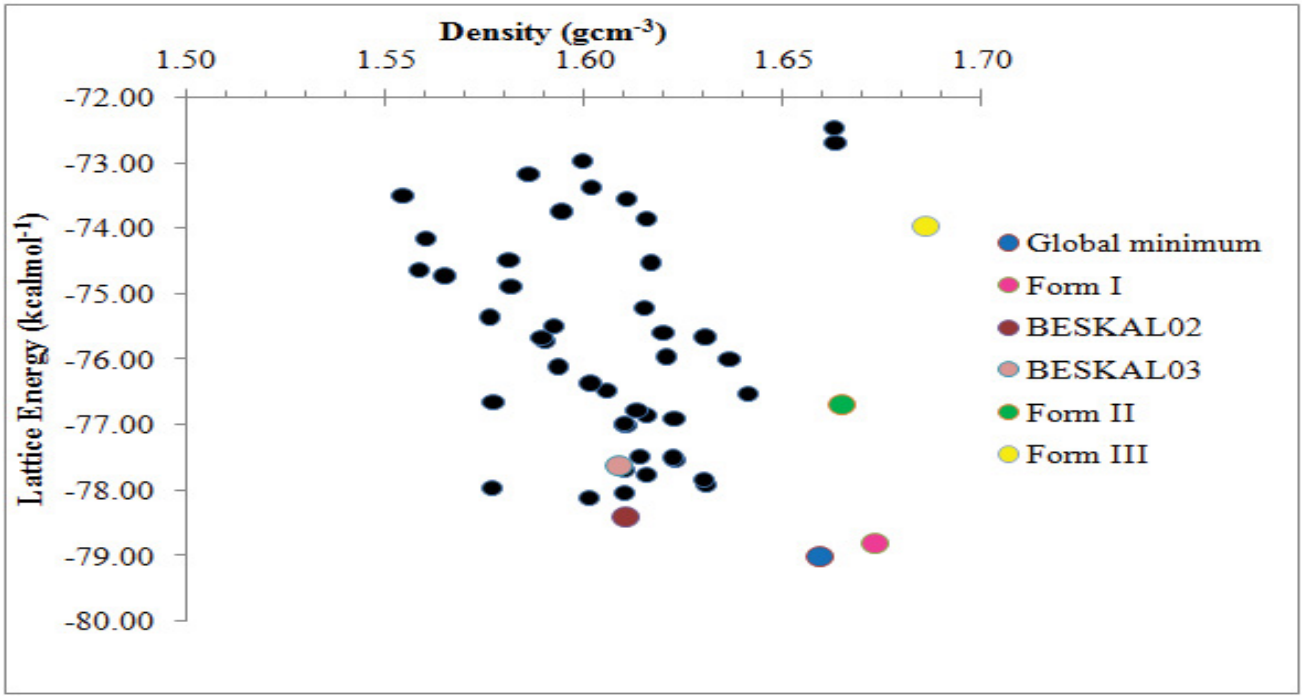

Figure 4) *Lattice energy landscape showing low energy and high density region encompassing experimentally observed three crystal forms of gentisic acid generated through CSP runs*

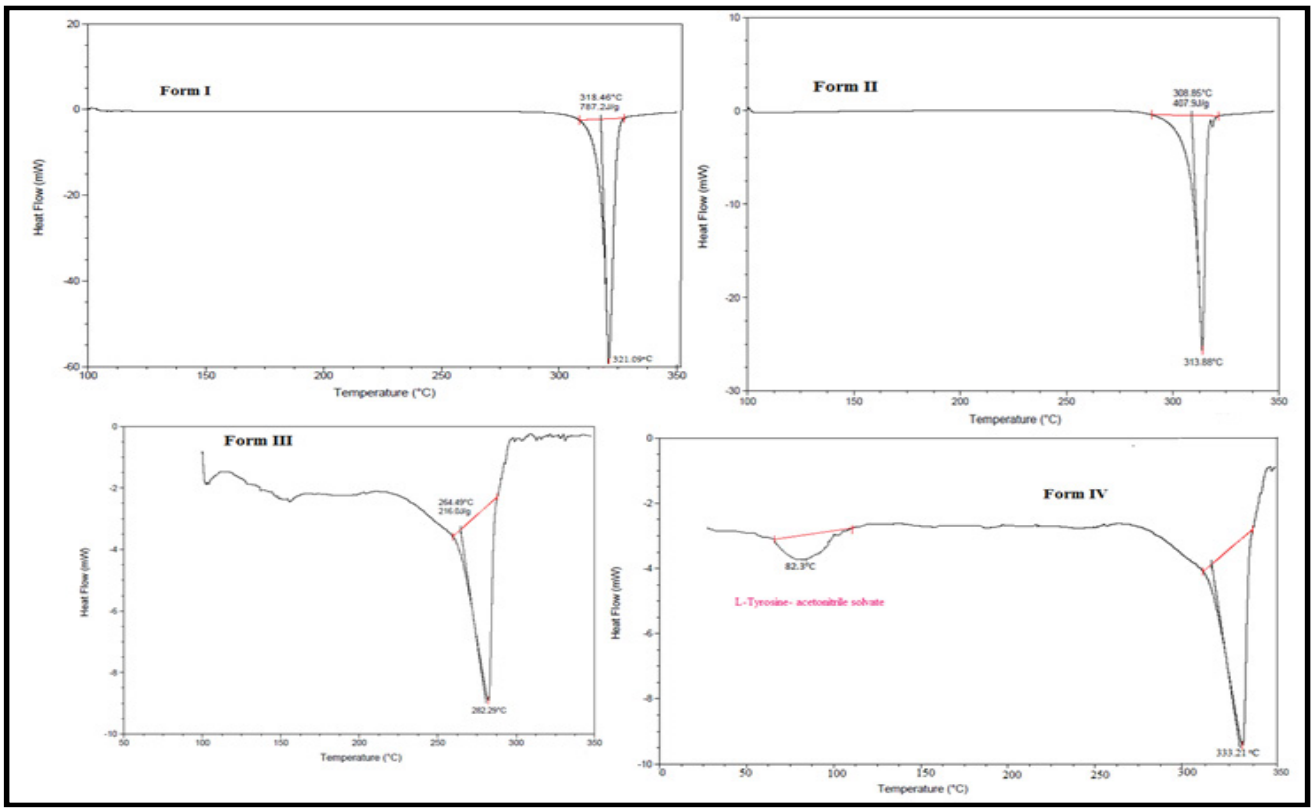

Figure 5) *DSC endotherms of various forms of L-tyrosine*

DSC patterns

The position of endotherms and DSC thermograms of various forms of gentisic acid and L-tyrosine are reported in Figures 2 and 5. In case of form IV of gentisic acid, a broad desolvation endotherm (at 79.94°C) appears prior to sharp melting endotherm (at 213.79 °C). TGA analysis of this form was undertaken which indicates a weight loss of 24.07% confirming it to be a solvatomorph i.e., formic acid solvate of gentisic acid with 1:1 stoichiometry (Figures 6-8). Similarly, form IV of L-tyrosine has shown a broad desolvation endotherm with maxima at 82.3°C. This form was further analysed through TGA which indicated a weight loss of 19.7% confirming it to be a solvatomorph i.e., acetonitrile solvate of L-tyrosine with 1:1 stoichiometry (Figure 7).

PXRD study

PXRD patterns of various forms of gentisic acid and L-tyrosine were observed carefully and are shown in Figures 8 and 9. The R_{wp}, a basic measure of

TABLE 4

CSP results of gentisic acid showing list of unique crystal structures ranked on the basis of the calculated lattice energy and density.

S .No	tructure Label	Space group	Density $_{gcm^{-3}}$	Lattice energy	a	b	C	Cell Parameters α β γ		
1	GA-3	C2/C	1.66	-79.01	23.92	4.73	13.21	90	124.78	90
2	GA-101	P-1	1.67	-78.80	11.92	9.39	5.12	74.98	94.80	106,80
3	GA-11	P21/C	1.61	-78.39	4.89	11.83	11.12		91.11	90
4	GA-21	P21	1.61	-78.04	6.70	13.43	3.64	90	75.97	90
5	GA-116	P212121	1.60	-78.12	7.03	6.21	14.63	90	90	90
6	GA-312	PBCA	1.58	-77.96	20.79	4.85	12.87	90	90	90
7	GA-172	C2/C	1.53	-77.91	27.58	4.75	13.19	90	133.35	90
8	GA-49	P212121	1.53	-77.83	5.05	24.57	5.03	90	90	90
9	GA-29	P-1	1.52	-77.75	5.91	4.78	10.52	105.32	104.01	72.17
10	GA-202	PBCA	1.51	-77.59	4.80	24.39	10.85	90	90	90
11	GA-169	P21/C	1.51	-77.51	5.57	4.79	23.82	90	100.21	90
12	GA-107	P212121	1.62	-77.54	10.11	4.82	12.94	90	90	90
13	GA-345	C2/C	1.62	-77.50	16.88	7.02	26.00	90	24.17	90
14	GA-488	P-1	1.61	-77.50	7.16	4.77	10.54	105.09	88.03	67.24
15	GA-160	PBCA	1.61	-77.00	24.35	10.86	4.81	90	90	90
16	GA-5	P21/C	1.51	-75.99	13.35	4.81	13.01	90	49.54	90
17	GA-183	P212121	1.52	-75.91	10.09	4.84	12.92	90	90	90
18	GA-441	P-1	1.52	-75.85	8.18	13.27	4.58	51.40	55.50	97.02
19	GA-247	C2/C	1.51	-75.78	19.65	7.03	14.57	90	140.91	90
20	GA-369	P21/C	1.57	-75.58	5.48	4.96	24.03	90	101.85	90
21	GA-193	PBCA	1.58	-75.56	20.66	4.86	12.92	90	90	90
22	GA-469	P-1	1.64	-75.54	7.08	9.85	8.28	84.42	120.22	135.91
23	GA-175	P21/C	1.61	-75.48	12.88	4.82	13.06	90	51.84	90
24	GA-9	PBCA	1.60	-76.36	25.18	10.55	4.81	90	90	90
25	GA-333	C2/C	1.59	-75.11	34.38	7.00	21.49	90	14.38	90
26	GA-446	C2/C	1.54	-75.00	14.03	7.01	14.50	90	51.30	90
27	GA-252	PBCA	1.52	-75.95	14.53	12.48	5.97	90	90	90
28	GA-173	P-1	1.59	-75.73	13.60	7.78	9.58	45.40	46.51	25.43
29	GA-159	P21/C	1.59	-75.58	11.44	4.84	12.81	90	65.28	90
30	GA-463	P21/C	1.53	-75.55	11.51	13.39	9.30	90	25.97	90
31	GA-339	C2/C	1.62	-75.59	13.00	4.82	20.74	90	76.28	90
32	GA-13	P-1	1.59	-75.49	8.55	7.74	6.92	119.18	53.59	105.16
33	GA-67	PBCA	1.58	-75.36	24.64	10.90	4.84	90	90	90
34	GA-354	P-1	1.62	-75.21	6.83	10.33	4.82	80.05	106.43	83.82
35	GA-63	P21/C	1.58	-74.90	7.14	20.30	4.85	90	55.90	90
36	GA-94	PBCA	1.57	-74.73	22.44	4.73	12.33	90	90	90
37	GA-8	C2/C	1.55	-74.64	21.97	4.75	12.80	90	100.25	90
38	GA-299	P-1	1.52	-74.53	5.84	11.79	4.81	71.50	105.11	119.55
39	GA-302	P21/C	1.58	-74.50	7.09	20.34	4.85	90	67.51	90
40	GA-404	C2/C	1.56	-74.16	22.03	4.75	12.77	90	79.29	90
41	GA-19	P21/C	1.69	-73.97	5.48	4.92	23.91	90	101.12	90
42	GA-133	P-1	1.62	-73.86	6.84	12.13	4.82	57.18	73.19	89.18
43	GA-491	C2/C	1.59	-73.75	15.49	7.02	14.54	90	53.74	90
44	GA-66	P21/C	1.51	-73.55	10.37	5.90	14.45	90	37.91	95

45	GA-45	C2/C	1.55	-71.51	23.40	4.72	12.82	90	111.70	90
46	GA-380	P21/C	1.50	-73.37	11.37	5.98	14.57	90	145.42	90
47	GA-36	C2/C	1.59	-73.18	12.20	7.47	14.93	90	108.35	90
48	GA-12	P21/C	1.50	-72.98	14.03	10.87	4.78	90	118.53	90
49	GA-22	P21/C	1.65	-72.70	7.77	12.63	7.91	90	127.58	90
50	GA-201	P21/C	1.65	-72.47	7.79	12.63	7.85	95	127.17	90
51	GA-20	C2/C	1.49	-72.13	4.96	13.02	9.53	90	90	90
52	GA-41	C2/C	1.45	-72.06	13.02	9.58	4.94	90	90	90
53	GA-89	P212121	1.53	-72.00	11.61	5.88	9.32	53.34	48.55	34.23
54	GA-4L0	PBCA	1.57	-71.79	11.65	5.90	9.31	53.24	48.83	33.94
55	GA-65	P212121	1.53	-71.18	13.23	8.27	11.99	90	90	90
56	GA-80	C2/C	1.57	-70.97	11.72	5.90	9.30	52.98	48.80	33.75
57	GA-51	P-1	1.64	-70.73	11.74	6.91	9.28	52.94	49.13	33.55
58	GA-28	P-1	1.64	-70.12	25.61	4.54	12.75	90	66.24	90
59	GA-92	PBCA	1.61	-69.80	7.66	13.29	12.66	90	90	90
60	GA-111	P-1	1.64	-69.20	11.87	6.95	9.24	52.47	49.45	32.97

TABLE 5

CSP results of L-tyrosine showing list of unique crystal structures ranked on the basis of the calculated lattice energy and density

S. no.	Structure Label	Space group	Density (gcm^{-3})	Lattice energy ($kcalmol^{-1}$)	a	b	c	α	β	γ
1	T-30	P212121	1.59	-27.8	21.16	4.5	7.07	90	90	90
2	T-21	C2/C	1.53	-27.3	9.07	20.97	6.93	90	91.01	90
3	T-6	PBCA	1.48	-26.9	11.52	29.2	5	90	91.01	90
4	T-15	PBCA	1.45	-26.66	29.19	5.01	11.52	90	90	90
5	T-20	P21	1.47	-26.21	12.59	7.45	5.33	90	119.52	90
6	T-27	P2/C	1.48	-26.01	11.26	4.94	15.42	90	103.76	90
7	T-23	P2/C	1.57	-25.81	5.26	6.94	21.41	90	104.87	90
8	T-11	P21	1.4	-25.23	12.59	7.5	5.3	90	119.67	90
9	T-16	P-1	1.46	-24.99	11.32	11.01	5.76	84.53	95.94	106.74
10	T-8	P-1	1.34	-24.58	15.97	4.87	7.65	97.15	73.93	132.76
11	T-1	P-1	1.35	-24.18	7.65	12.19	4.86	90.78	97.05	111.51
12	T-17	P-1	1.43	-23.77	7.71	12.07	4.9	89.82	98.35	111.17
13	T-9	P212121	1.37	-23.23	10.32	9.27	8.98	90	90	90
14	T-7	PNA21	1.33	-22.99	9.74	8.67	10.4	90	90	90
15	T-3	C2/C	1.31	-22.28	15.67	5.02	23	90	70.49	90
16	T-44	P212121	1.35	-21.88	4.73	9.24	19.42	90	90	90
17	T-57	P212121	1.43	-21.55	4.73	9.24	19.44	90	90	90
18	T-86	P21/C	1.42	-21.3	9.32	7	12.72	90	82.81	90
19	T-155	P212121	1.27	-21.27	11.4	5.21	14.73	90	90	90
20	T-208	P212121	1.28	-21.22	5.93	28.49	5.02	90	90	90
21	T-271	P21	1.31	-21.1	10.52	6.34	6.53	90	106.51	90
22	T-236	P21	1.28	-20.84	10.7	6.33	6.54	90	70.53	90
23	T-117	P212121	1.43	-20.58	6.88	15.29	8.27	90	90	90
24	T-169	C2/C	1.3	-20.34	15.68	4.94	22.6	90	70.53	90
25	T-89	PBCA	1.43	-20.19	11.3	32.42	4.71	90	90	90
26	T-10	P21	1.4	-19.97	10.56	7.26	5.53	90	84.86	90
27	T-176	P21	1.43	-19.53	10.57	7.23	5.55	90	85.04	90
28	T-99	P21	1.43	-19.19	10.56	7.26	5.52	90	84.94	90
29	T-75	P21	1.41	-18.95	12.33	7.17	5.58	90	121.11	90

30	T-300	P21	1.41	-18.79	5.49	7.3	12.29	90	121.14	90
31	T-430	P21/C	1.37	-18.77	7.82	22.66	8.67	90	146.62	90
32	T-218	P21/C	1.42	-18.74	5.99	17.38	8.38	90	82.56	90
33	T-456	C2/C	1.41	-18.71	11.13	4.97	29.96	90	87.2	90
34	T-5	PBCA	1.37	-18.57	8.72	10.44	18.79	90	90	90
35	T-22	PBCA	1.45	-20.58	8.72	10.44	18.79	90	90	90
36	T-39	P21/C	1.45	-20.34	10.9	17.2	8.44	90	33.1	90
37	T-26	PBCA	1.39	-20.19	15.24	23.7	4.95	90	90	90
38	T-112	PBCA	1.39	-19.97	15.25	23.7	4.95	90	90	90
39	T-482	P2/C	1.3	-19.53	11.85	4.9	15.57	90	109.85	90
40	T-68	P2/C	1.21	-19.19	16.07	4.9	23.6	90	152.75	90
41	T-13	P21/C	1.3	-18.95	4.84	20.19	9.18	90	65.58	90
42	T-154	P21/C	1.32	-18.79	4.83	20.2	9.19	90	65.48	90
43	T-92	P21/C	1.4	-18.77	4.85	22.8	7.9	90	102.98	90
44	T-71	P21	1.4	-18.74	11.9	5.05	7.32	90	99.42	90
45	T-333	P21	1.38	-18.71	7.31	5.05	11.91	90	99.47	90
46	T-261	P21	1.36	-18.57	14.96	5.06	7.31	90	51.8	90
47	T-421	P21	1.41	-18.53	8.21	5.32	10.44	90	112.92	90
48	T-63	P-1	1.41	-18.5	4.53	10.89	9.12	94.25	78.28	77.36
49	T-344	P21/C	1.36	-18.46	10.75	6.37	12.84	90	71.4	90
50	T-203	P21/C	1.43	-18.43	19.19	6.43	12.75	90	31.97	90
51	T-217	P21	1.39	-18.41	5.87	5.23	13.63	90	89.06	90
52	T-483	P21	1.39	-18.38	8.66	7.92	6.14	90	89.49	90
53	T-361	P21	1.38	-18.35	6.14	7.93	10.67	90	54.19	90
54	T-160	PBCA	1.4	-18.3	11.73	30.21	5.02	90	90	90
55	T-398	P-1	1.4	-18.26	4.83	11.35	9.07	67.29	65.94	72.2
56	T-410	P-1	1.26	-18.22	8.36	11.35	4.83	72.26	82.13	104.03
57	T-119	C2/C	1.34	-18.16	16.74	14.68	12.48	90	147.42	90
58	T-95	C2/C	1.41	-18.12	16.73	14.68	9.15	90	132.71	90
59	T-77	P-1	1.4	-18.1	9.32	7.2	8.7	46.74	76.04	84.18
60	T-53	P-1	1.37	-17.95	7.29	9.15	6.6	78.57	103.8	84.91

TABLE 6

Melting point (°C) and DSC endotherms (°C) of gentisic acid polymorphs/solvatomorph

Polymorphs/solvatomorph	M.pt. (°C)	DSCendotherm (°C)	
		Desolvation	Melting
Commercial sample	206- 208	-	207.13
Form I	211- 213	-	211.72
Form II	202- 204	-	203.55
Form III	196-198	-	197.64
Form IV	212- 215	79.94	213.79

similarity between a simulated and an experimental diffraction pattern of each candidate crystal structure is found out to be below 15%, which indicates that there is good agreement between crystal structure solution done by MS and experimental crystal structures (Figures 10 and 11) in both the selected cases.

FTIR spectroscopy

The various forms of chosen drugs had shown certain variations in their frequency bands as shown in their FTIR spectra (Figures 12 and 13). The characteristic frequencies are listed in Tables 8 and 9. These variations in the FTIR spectra indicated the changes in the intermolecular interactions within these modifications.

Crystal structure determination from PXRD patterns

The detailed analysis of crystals of the selected drug molecules generated from solution of their PXRD patterns by MS along with the interpretation of CSP results by exploring the developed forms in the lattice energy landscape was attempted systematically.

Detailed analysis of crystal structures of gentisic acid

Crystal form in commercial sample (CCDC code- BESKAL 02): This form is reported in literature and its single crystal X-ray diffraction analysis has already been done. It crystallizes out in monoclinic form with P-21/c space group with four molecules of gentisic acid in a unit cell (Figure 14b). The

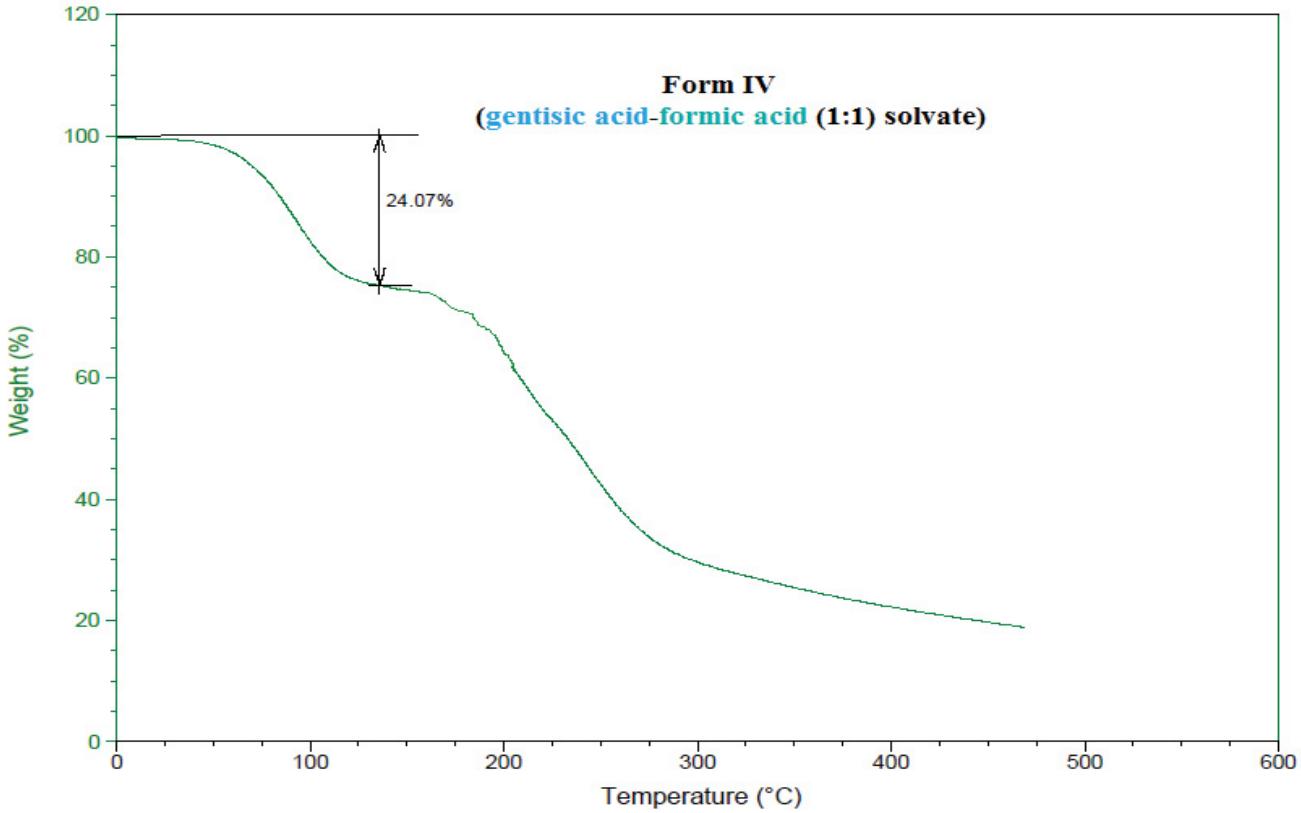

Figure 6) *TGA scan of formic acid solvate (form IV) of gentisic acid*

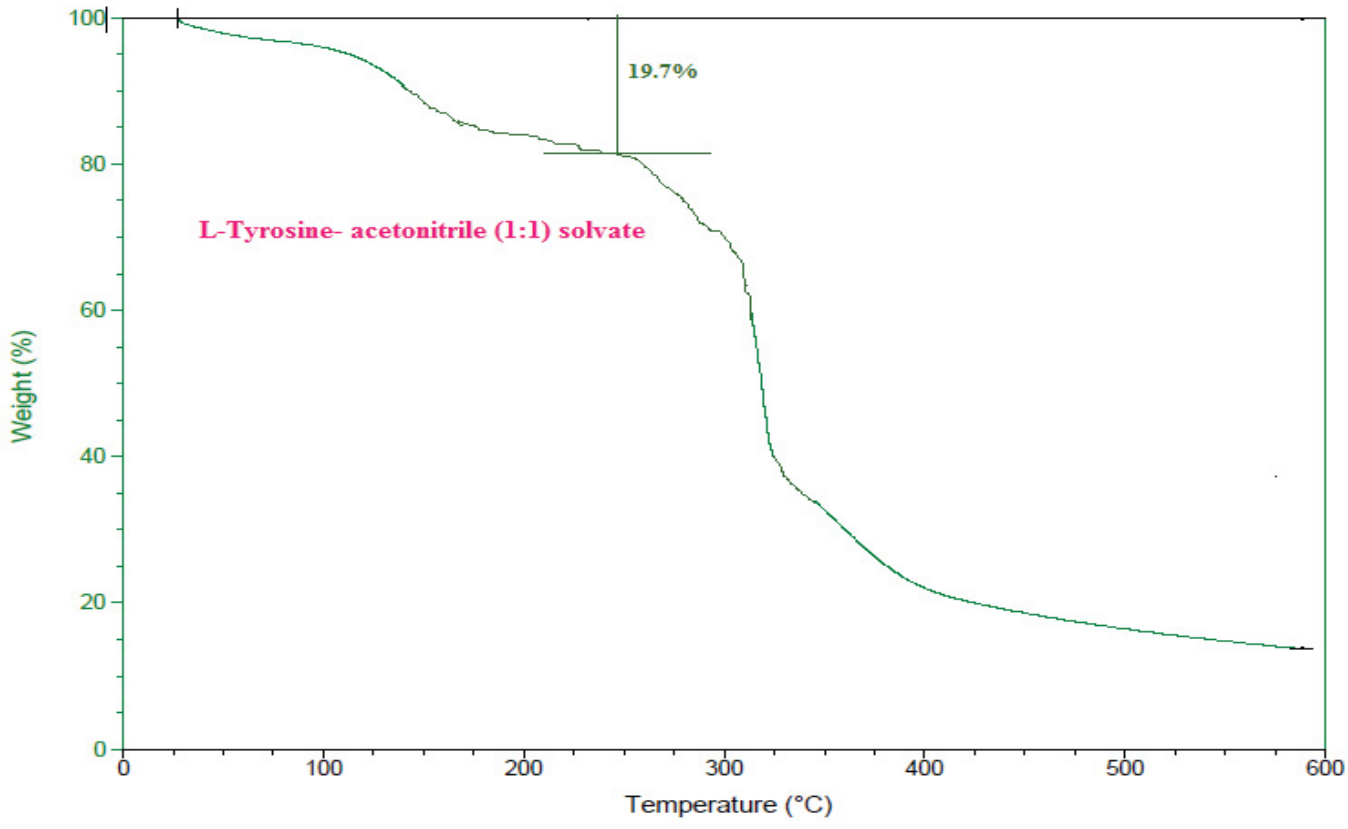

Figure 7) *TGA scan of acetonitrile solvate (form IV) of L-tyrosine*

molecules are arranged in two different planes in such a way that the adjascent molecules form an angle of 79.64° w. r. t. each other. The molecular packing diagram (Figure 14c) clearly shows that one molecule is attached to four other molecules through intermolecular hydrogen bonding interactions. Symmetry-independent molecules aggregate via the carboxylic acid dimer i.e. O(3)H···O(4). It is also found out that phenolic group i.e. O(1)H and O(2)H of one molecule are hydrogen bonded with phenolic oxygen i.e. O(2) and O(1) of other two molecules respectively i.e. O(1)H···O(2) and O(2)

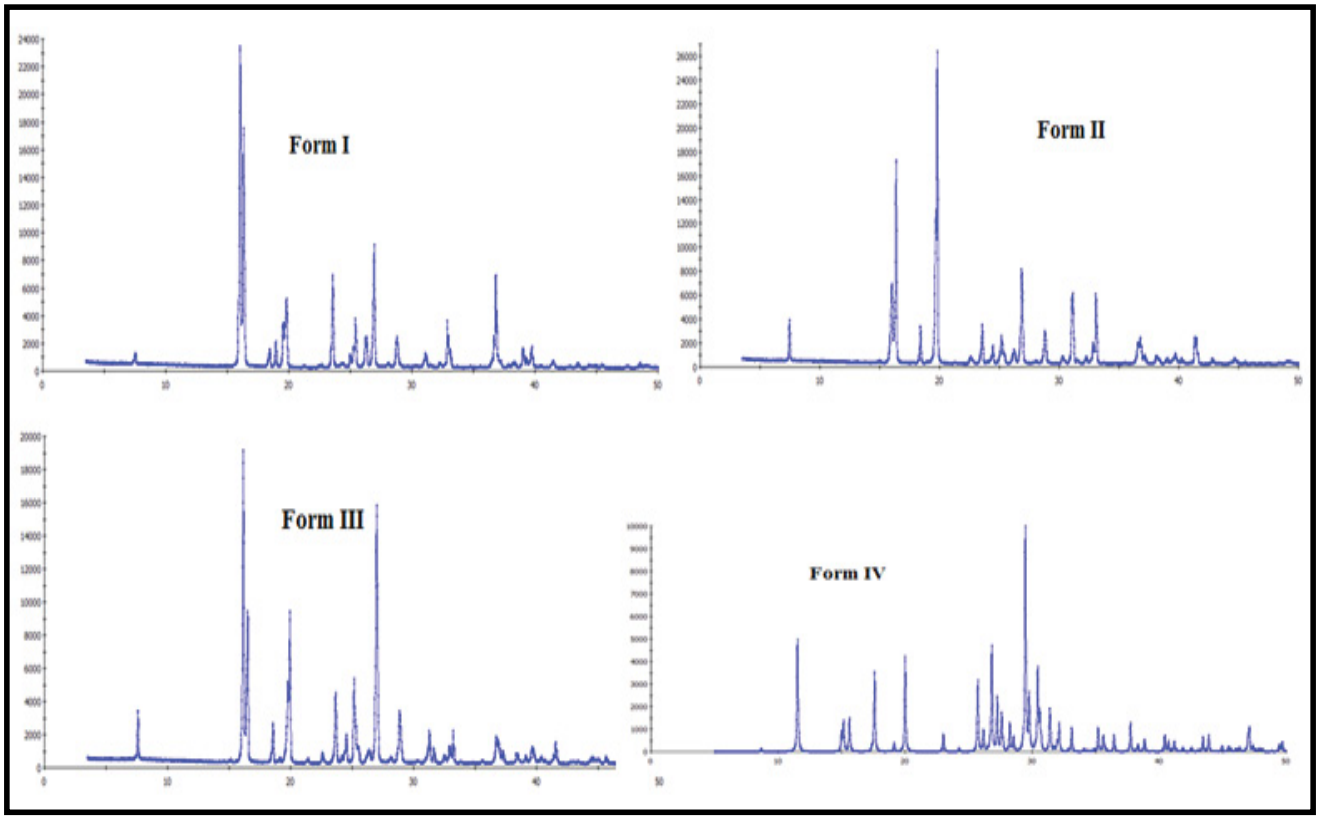

Figure 8) *PXRD patterns of various forms of gentisic acid*

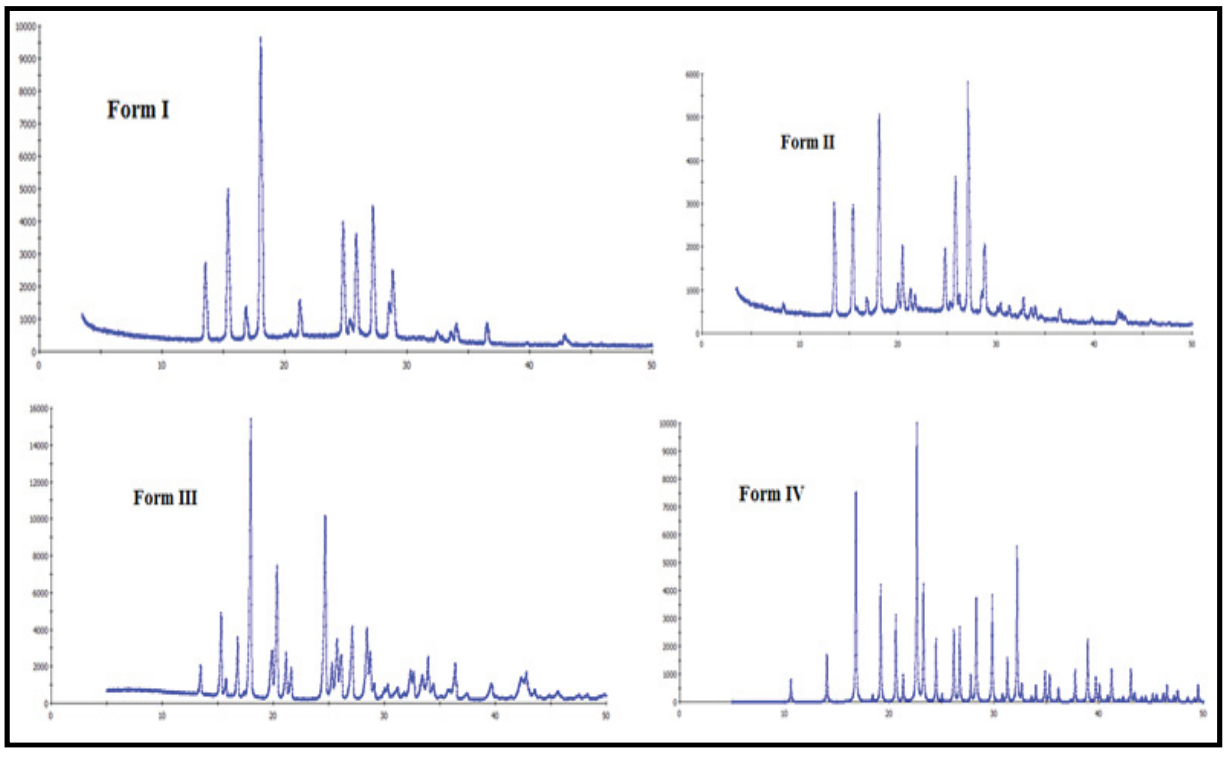

Figure 9) *PXRD patterns of various forms of L-tyrosine*

H···O(1). The detailed packing network in 3-D view indicates stacked layers of molecules running in anti-parallel sequence (Figure 14d).

Form I

The crystal structure analysis of this form demonstrates that it crystallises in triclinic form with P-1 space group with two molecules of gentisic acid in a unit cell (Figure 15b). The molecules are confined in single plane in head to tail pattern in such a way that one molecule is joined to other through hydrogen bonding between phenolic oxygen O(2) of one molecule and hydrogen of carboxyl group of next molecule i.e. O(3)H···O(2) (Figure 15c). The detailed packing network in 3-D view indicates stacked layers of molecules in the form of sheet (Figure 15d).

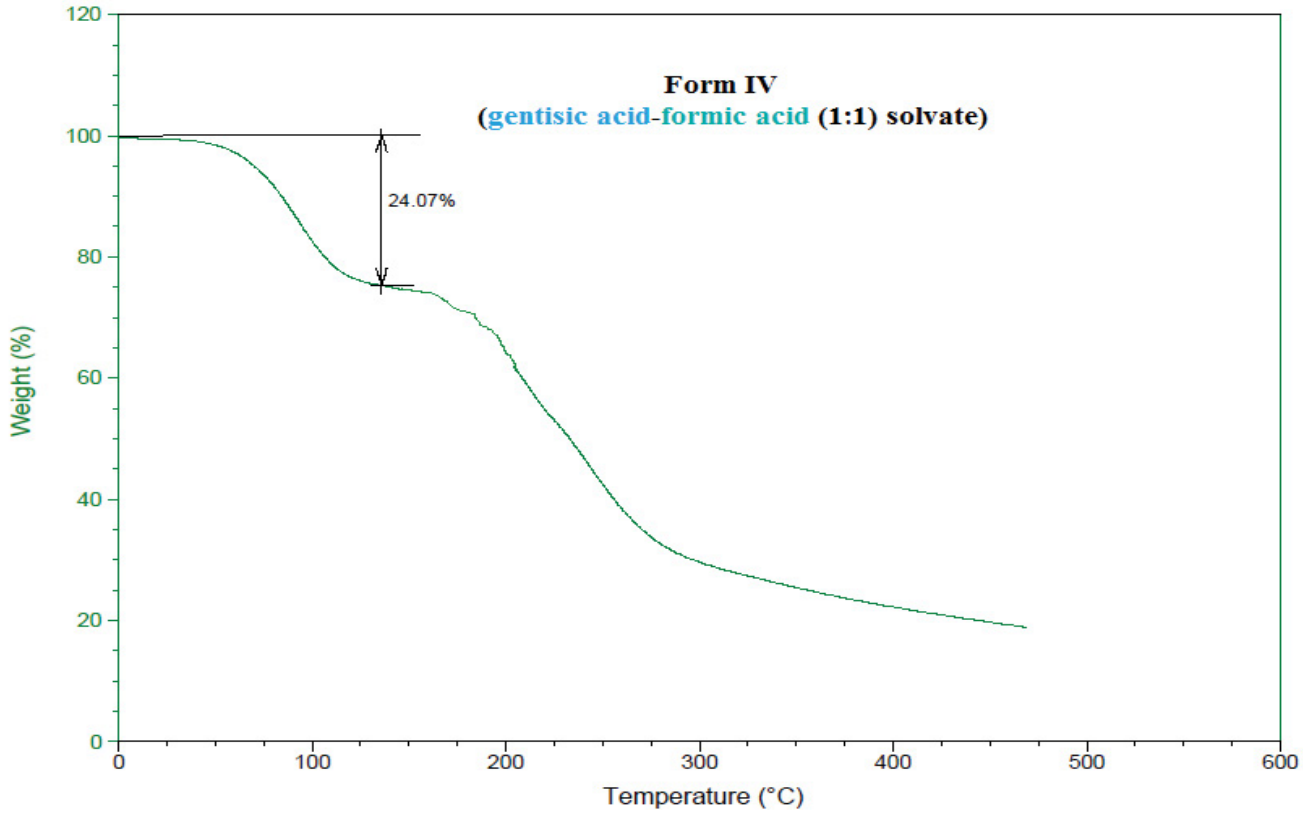

Figure 10) *Comparison of the experimental and simulated powder patterns of the observed four forms of gentisic acid*

TABLE 7
Melting point (°C) and DSC endotherms (°C) of L-tyrosine polymorphs/solvatomorph

Polymorphs/ solvatomorph	M.pt. (°C)	DSC endotherm (°C)	
		Desolvation	Melting
Form I	320- 322	-	321.09
Form II (commercial sample)	312- 315	-	313.88
Form III	282- 284	-	282.29
Form IV (acetonitrile solvate)	332- 334	82.3	333.21

Form II

This form consists of four molecules enclosed in a unit cell which is in monoclinic in nature with P-21/c space group. (Figure 16b). The molecules are arranged in two different planes in such a way that the adjascent molecules form an angle of 58.76° w. r. t. each other. The packing diagram of this form clearly indicates that one molecule is joined to two other molecules (Figure 16c). The hydrogen bonding pattern of this form displays both intermolecular and intramolecular hydrogen bonds. The oxygen (O(4)) of the carboxyl group is pointed in such a way that it forms intramolecular and intermolecular hydrogen bonds with hydrogens of carboxyl groups in the same and different molecules respectively i.e. O(3)H···O(4). The detailed packing network in 3-D view indicates stacked chains of adjascent molecules in a criss-cross fashion running in an anti-parallel sequence w.r.t. next chain of adjascent molecules (Figure 16d).

Form III

This form emerges in monoclinic crystal system with P-21/c space group with four molecules of gentisic acid in a unit cell (Figure 17b). The molecules are arranged in two different planes in such a way that the adjascent molecules form an angle of 85.22° w. r. t. each other. The molecular packing diagram of this modification (Figure 17c) manifests that each molecule is further joined to seven other molecules through intermolecular hydrogen bonds forming corrugated aggregates. The hydrogen bonds on phenolic group (O(1)H and O(2)H) are found to be bifurcated by acting both as hydrogen bond donors and acceptors i.e. O(3)H···O(1)H···O(4) and O(2)H···O(2)H···O(2) respectively. The hydrogen of the carboxyl group i.e. O(3)H is simultaneously involved in hydrogen bonding interaction with oxygen of carboxyl group (O(4)) of one molecule and phenolic oxygen (O(1)H) of another molecule. The detailed packing network in 3-D view indicates two stacked layers of molecules in a criss-cross fashion placed upside down w.r.t. each other (Figure 17d).

Form IV

This monoclinic crystal system of this form with P-21/c space group consists of four molecules each of gentisic acid and formic acid with P-21/c space group in a unit cell (Figure 18b). The molecules are confined in single plane. All the oxygen atoms of a molecule are engaged in forming hydrogen bonds with adjascent molecules including solvent molecules (formic acid). It is clearly shown in packing diagram (Figure 18c) of this solvatomorph that each solvent molecule is shared by three gentisic acid molecules through intermolecular hydrogen bonds. The hydrogen bonds associated with

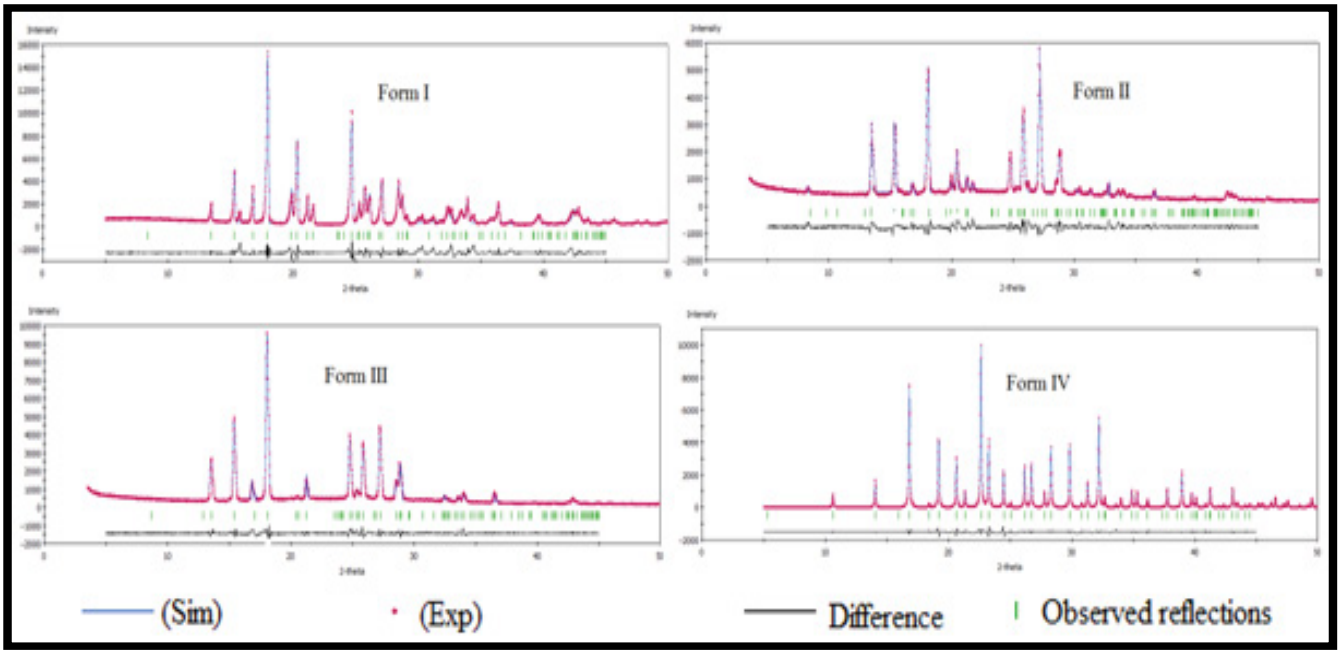

Figure 11) *Comparison of the experimental and simulated powder patterns of the observed four forms of L-tyrosine*

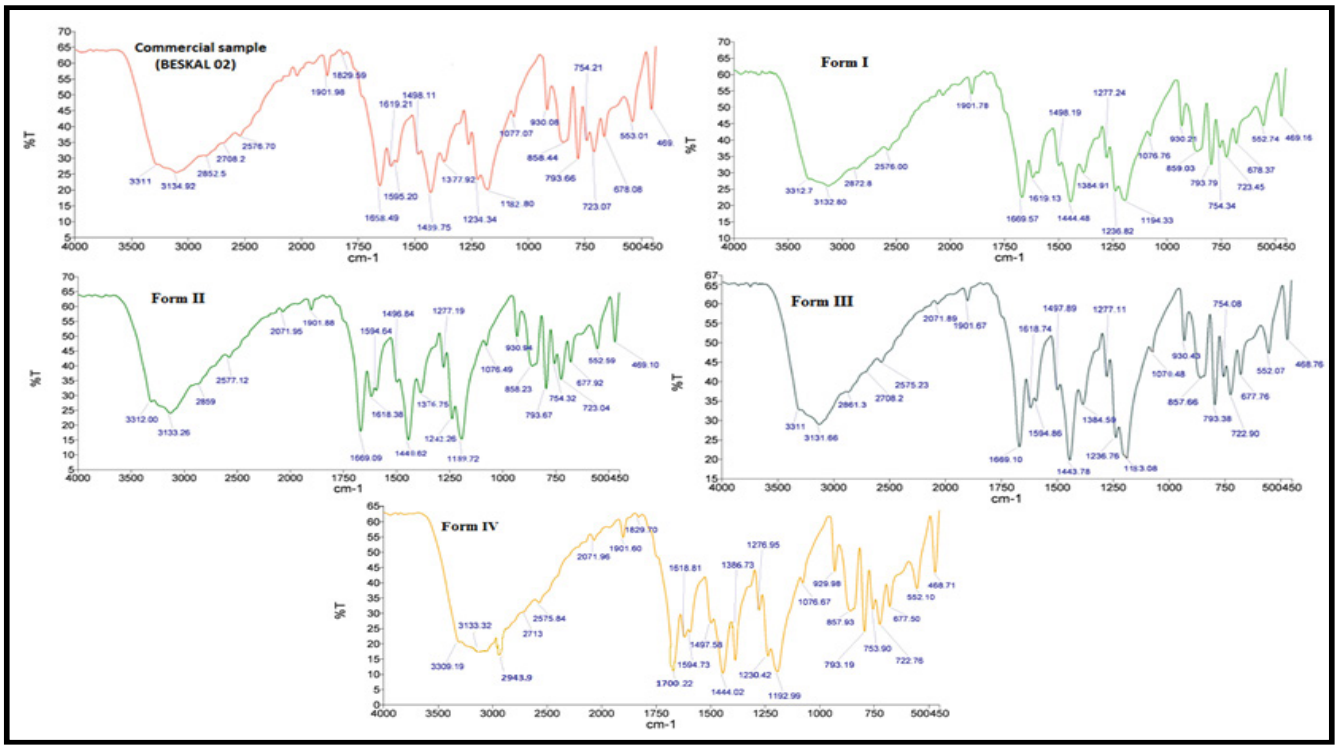

Figure 12) *FTIR spectra of various forms of gentisic acid*

hydroxyl (O(5)H) of carboxylic group of formic acid are bifurcated i.e. O(1) H···O(5)H···O(1). On the other hand, the oxygen of carboxylic group of formic acid (O(6)) is joined to the hydrogen of the phenolic group (O(2)H) of gentisic acid. Besides this the hydrogen bonding pattern shown in Figure 16c clearly depicts that each gentisic acid molecule further directly joined with itself and with two other gentisic acid molecules through intramolecular and intermolecullar hydrogen bonds respectively. The intramolecular bond is present between hydrogen of phenolic group (O(1)H) and oxygen of carboxyl group (O(4)) of same gentisic acid molecule. The intermolecular hydrogen bonding is well exhibited between two gentisic acid molecules via hydrogen of the carboxylic group (O(3)H and oxygen of phenolic group (O(2) H) i.e., O(3)H···O(2). The detailed packing network in 3-D view indicates the molecules are arranged in form of stacked chains in a zig-zag manner with solvent molecules trapped inside them (Figure 18d).

The various polymorphs observed experimentally along with the two forms reported in literature (with CCDC Refcode: BESKAL02 and 03) [24,25] were located among the fifty predicted unique (with low energy and high density) crystal structures of gentisic acid (Table 4). The structure no. 2, 20 and 41 were matched well with experimentally observed forms whereas structures 3 and 11 corresponds to BESKAL 02 and 03 respectively. The commercial sample matches well with BESKAL02. However these were not the lowest energy calculated structures. They were found within an energy difference of approximately 7.0 kcal/mol. The lattice energy diagram is shown in Figure 17 in which the experimentally matched forms were highlighted with different colors (mentioned under legend). The other forms reported in literature (with space group P21/a, other with space group Pa with CCDC Refcode:

TABLE 8

Prominent peaks of gentisic acid polymorphs in FTIR spectra

Functional group assignment	FTIR Peaks (cm^{-1})				
	Commercial sample	Form I	Form II	Form III	Form IV*
Saturated C-H stretch	2852.5	2872	2859	2861.3	2943.9
O-H bending vibrations	1439.75	1444.48	1440.62	1443.78	1444.02
C–O stretch	1377.92 and 1234.34	1384.91and 1236.82	1376.75 and1242.26	1384.59 and1236.76	1386.73 and 1230.42
C-O-C stretch	1188.80	1194.33	1189.72	1183.08	1192.99
Aromatic C-H bend	1082.80	1076.76	1076.49	1070.48	1076.67

TABLE 9

Prominent peaks of L- tyrosine polymorphs in FTIR spectra

Functional group assignment	FTIR Peaks (cm^{-1})			
	Form I	Form II#	Form III	Form IV*
N-H bending modes of $–NH_2$	1595, 1157 and1101	1589.8, 1150 and1107	1583, 1162 and1103	1589.8, 1150 and1107
N-C stretch	1041	1047	1051	1047
phenolic C–O stretch	1244	1250	1248	1250
CH_2 bending modes	1451 and1101	1457 and1107	1462 and1103	1457 and1107
CH_3 stretch	-	-	-	2957 and 3009
CN stretch	-	-	-	2268

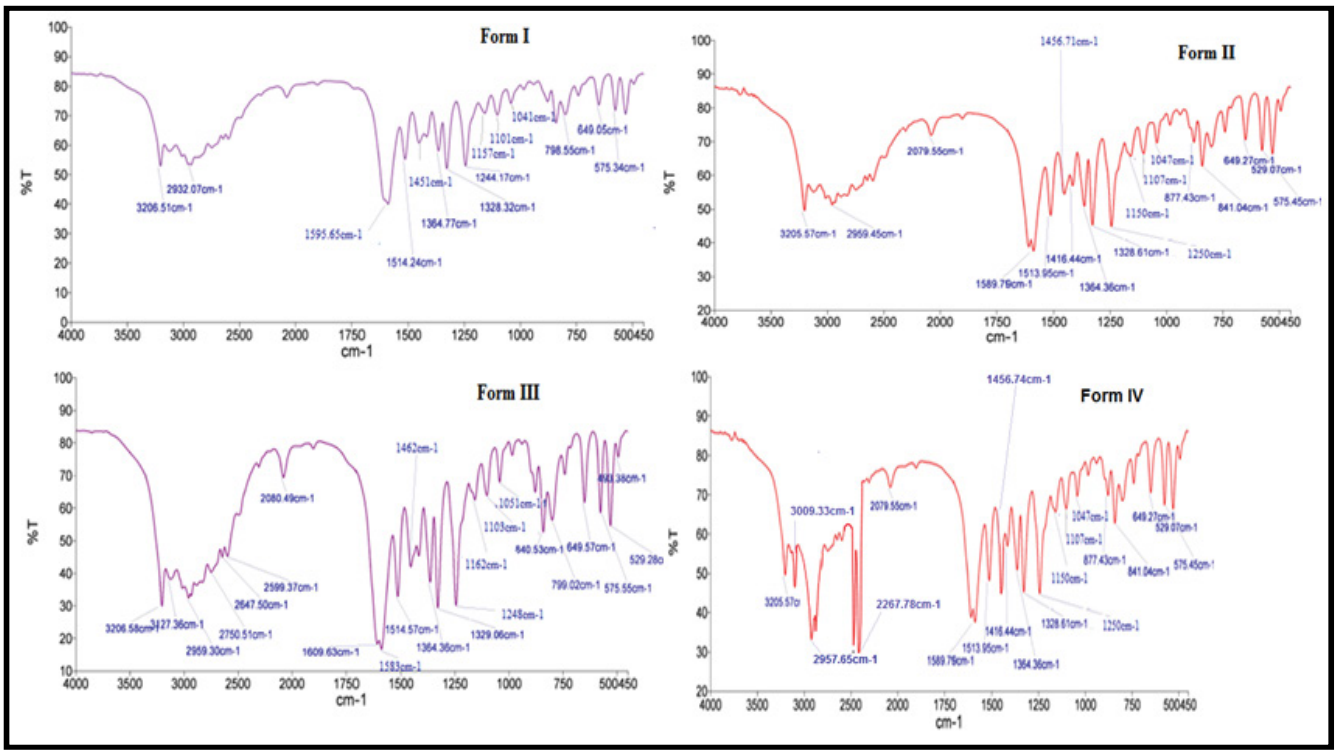

Figure 13) *FTIR spectra of various forms of L-tyrosine*

BESKAL01 (Z′=2) and rest five forms with space group P21/n with CCDC Refcode: BESKAL08- 09) [24,25] is beyond the scope of material studio to recognize them.

Detailed analysis of crystal structures of L-tyrosine

Form I

The crystal structure analysis of this form shows that it crystallizes in monoclinic form with P-C2/C space group with eight molecules of L-tyrosine in a unit cell (Figure 19b). The molecules are arranged in two different planes inclined at an angle of 31.89° and linked with each other through intermolecular hydrogen bonds. Each tyrosine molecule is connected to four other tyrosine molecules shown in (Figure 19c). The hydrogen of the carboxyl group is attached to nitrogen of the amino group and oxygen (O(3)) of the carboxyl group is linked to hydrogen of the phenolic group (O(2)H). Furthermore it is noticed that hydrogen of amino group is attached to oxygen of the phenolic group i.e. N(1)H···O(2). The detailed packing network in 3-D view indicates zig-zag and coiled chain like pattern of molecules (Figure 19d).

Form II

This form appears in orthorhombic shape with P-212121 space group having four molecules of L-tyrosine in a unit cell (Figure 20b). The molecules are arranged in two different planes inclined at an angle of 19.63° and linked with each other through intermolecular hydrogen bonds. The hydrogen bonding pattern (Figure 20c) clearly depicts that each tyrosine molecule is attached to four other tyrosine molecules forming a tetramer. The amino group is completely engaged in hydrogen bonding. Its one hydrogen forms bond with carboxylic oxygen of one tyrosine molecule i.e. N(1)H···O(1), other is connected to phenolic oxygen of other tyrosine molecule i.e. N(1) H···O(2) and nitrogen of it is bonded to hydrogen of phenolic group of other tyrosine molecule i.e. O(2)H···N(1). i.e., O(1)H···O(2). The phenolic oxygen is simultaneously forming hydrogen bonds with hydrogen of amino group as discussed before and also with hydrogen of carboxylic group i.e., O(1) H···O(2). The detailed packing network in 3-D view indicates chicken wire mesh forming criss-cross pattern of molecules (Figure 20d).

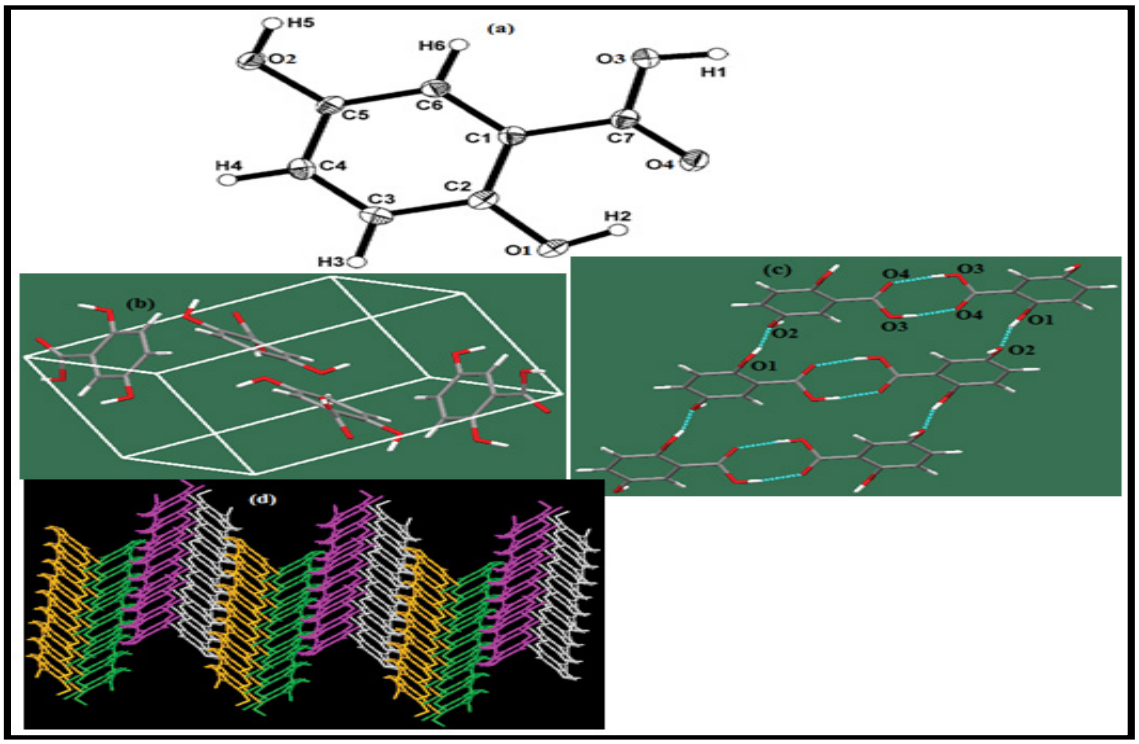

Figure 14) *Crystal structure analysis of form present in commercial sample (CCDC code- BESKAL 02) of gentisic acid- (a) Ortep diagram of asymmetric unit with 50% thermal ellipsoid probability. (b) arrangement of molecules in unit cell. (c) Hydrogen bonding patterns. (d) Molecular packing diagram (3-D network) along a-axis*

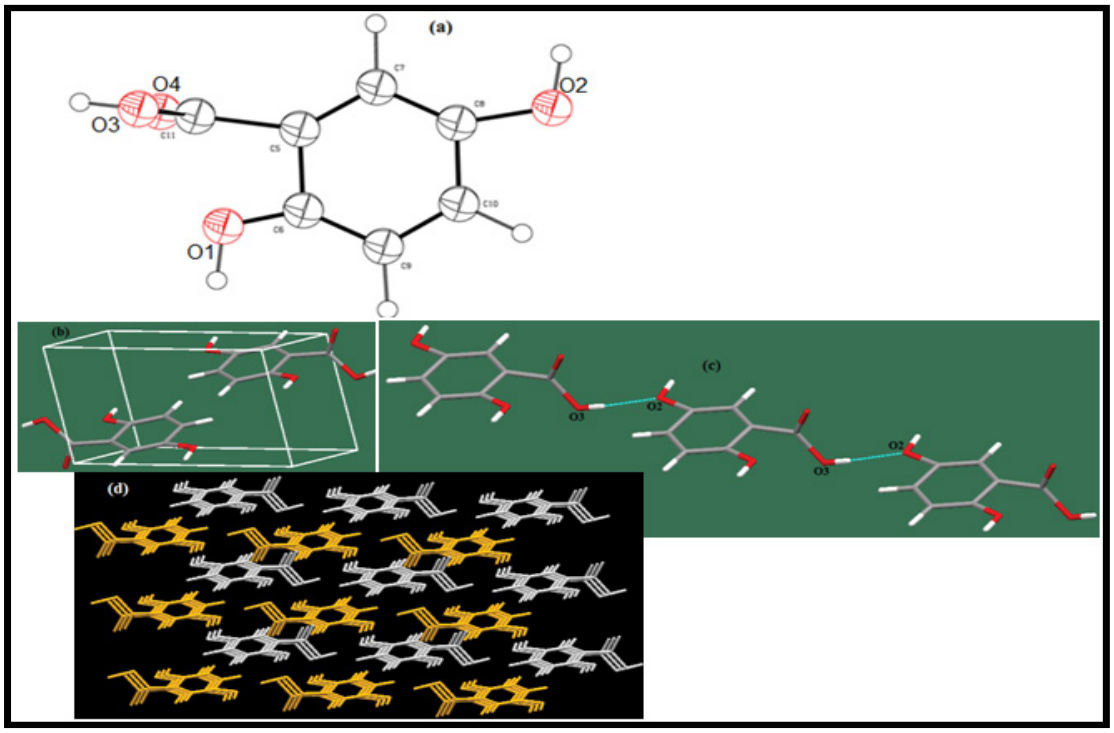

Figure 15) *Crystal structure analysis of form I of gentisic acid- (a) Ortep diagram of asymmetric unit with 50% thermal ellipsoid probability. (b) arrangement of molecules in unit cell. (c) Hydrogen bonding patterns. (d) Molecular packing diagram (3-D network) along a-axis*

Form III

The crystal structure analysis of this form demonstrates that it originates in orthorhombic form with P-2/c space group with four molecules of L-tyrosine in a unit cell (Figure 21b). The molecules are arranged in two different planes inclined at an angle of 70.13° and linked with each other through intermolecular hydrogen bonds. Each tyrosine molecule is further connected to three other molecules (Figure 21c). The hydrogen bonding pattern of this modification reveals the existence of carboxylate dimer i.e. O(1)H···O(3). The amino nitrogen acts as hydrogen bond acceptor forming bond with hydrogen of phenolic group i.e. O(2)H···N(1). The detailed packing network in 3-D view indicates stacked chains of molecules running in anti-parallel sequence (Figure 21d).

Form IV

This solvatomorph crystallizes in orthorhombic geometry with P-212121 space group with four molecules each of L-tyrosine and acetonitrile in a unit cell (Figure 22b). All the molecules are set at three different angular dispositions i.e. 44.58°, 37.21° and 59.42° w. r. t. each other. The molecular

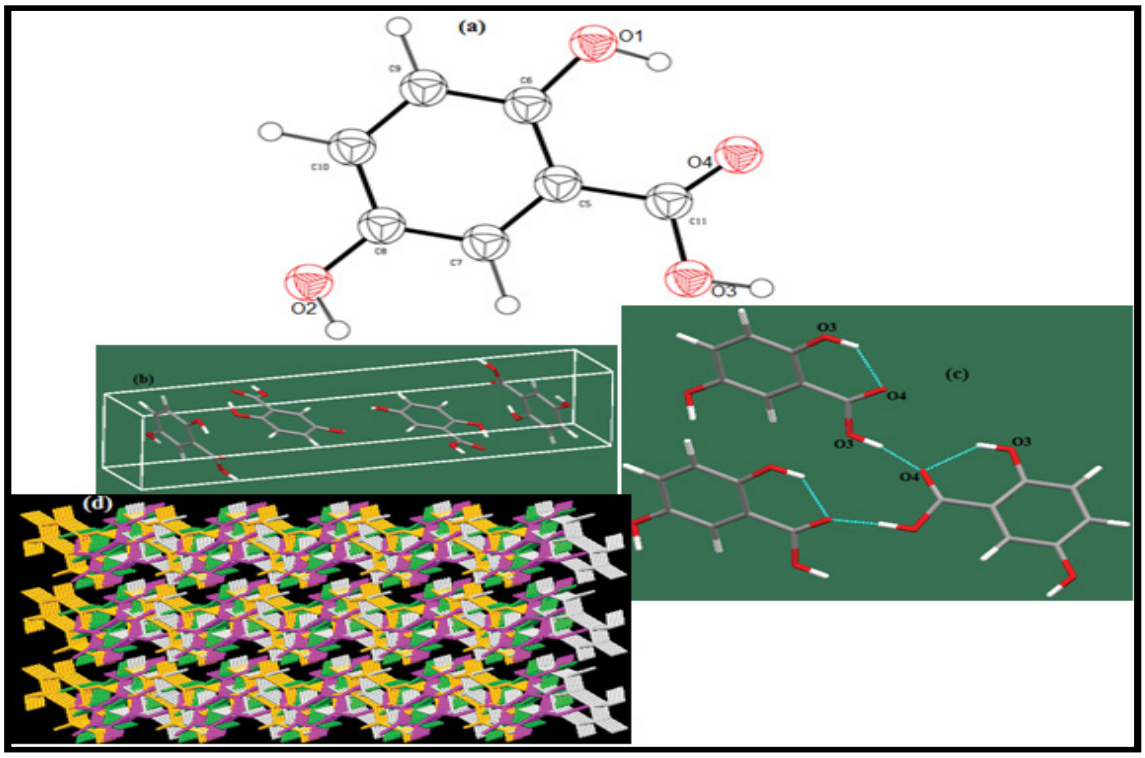

Figure 16) *Crystal structure analysis of form II of gentisic acid- (a) Ortep diagram of asymmetric unit with 50% thermal ellipsoid probability. (b) arrangement of molecules in unit cell. (c) Hydrogen bonding patterns. (d) Molecular packing diagram (3-D network) along a-axis*

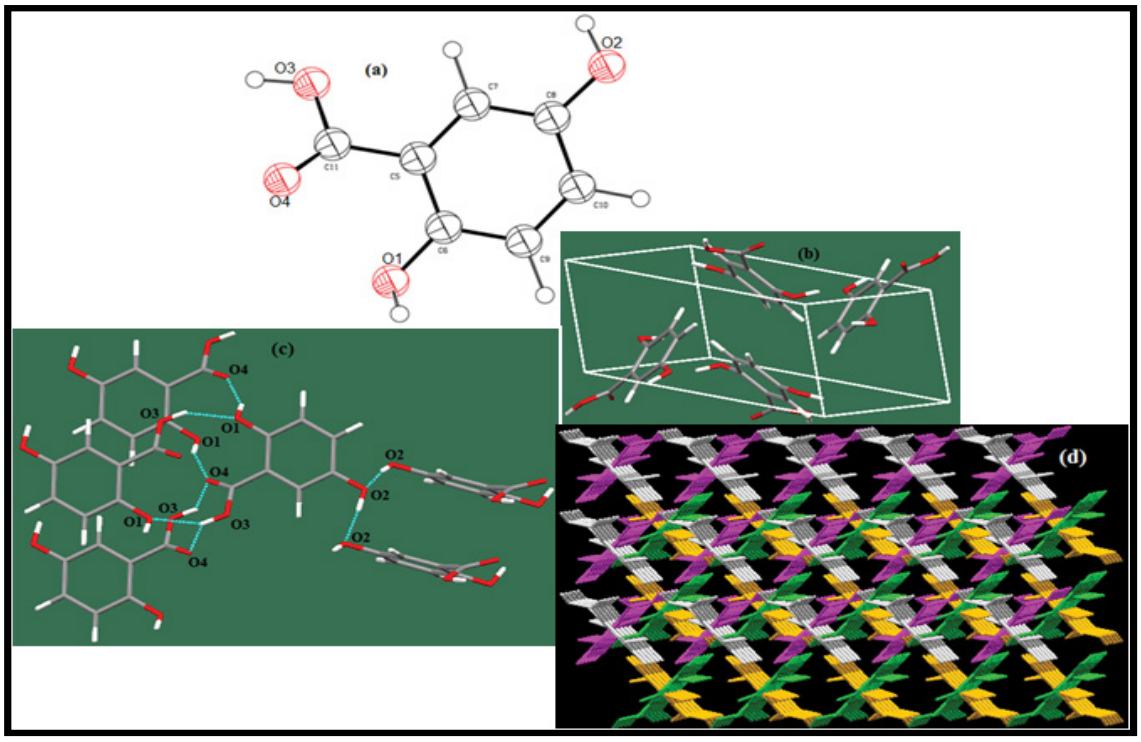

Figure 17) *Crystal structure analysis of form III of gentisic acid- (a) Ortep diagram of asymmetric unit with 50% thermal ellipsoid probability. (b) arrangement of molecules in unit cell. (c) Hydrogen bonding patterns. (d) Molecular packing diagram (3-D network) along a-axis*

packing diagram (Figure 22c) depicts that each molecule of tyrosine interacts with two other molecules and also with solvent (acetonitrile) molecule through intermolecular hydrogen bonding. It is quite clear from the hydrogen bonding schemes that acetonitrile nitrogen (N(2)) acts as hydrogen bond acceptor and is bonded to hydrogen of the amino group on tyrosine i.e. N(1)H···N(2). Besides this hydrogen of carboxylic group is associated with nitrogen of amino group of other molecule i.e. O(1)H···N(1) and oxygen of carboxylic group is linked to hydrogen of phenolic group on other molecule i.e. O(2)H···O(3). There is 3-D network of molecules forming a web like structure in which solvent molecules are entrapped (Figure 22d).

The crystal structures observed experimentally were located among the fifteen predicted unique (with low energy and high density) crystal structures of L-tyrosine (Table 5). The structure no. 1, 2 and 7 were matched well with experimentally observed forms. The commercial sample matches well with

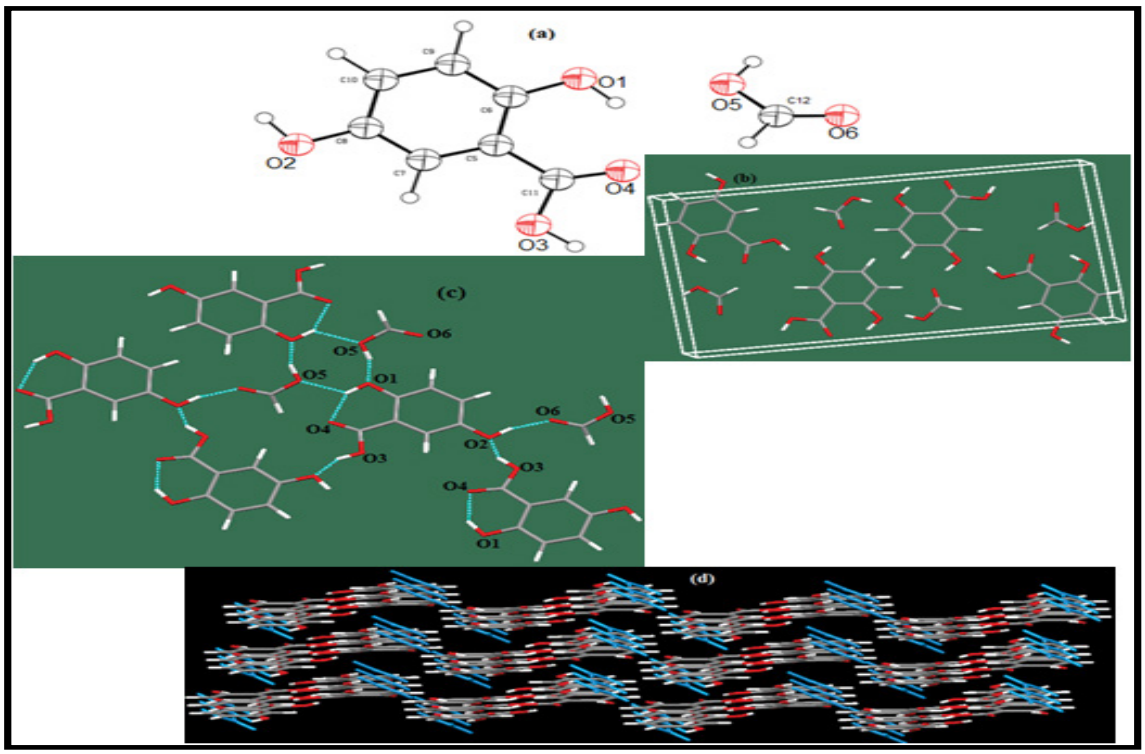

Figure 18) *Crystal structure analysis of form IV of gentisic acid (formic acid solvate)- (a) Ortep diagram of asymmetric unit with 50% thermal ellipsoid probability. (b) arrangement of molecules in unit cell. (c) Hydrogen bonding patterns. (d) Molecular packing diagram (3-D network) along a-axis*

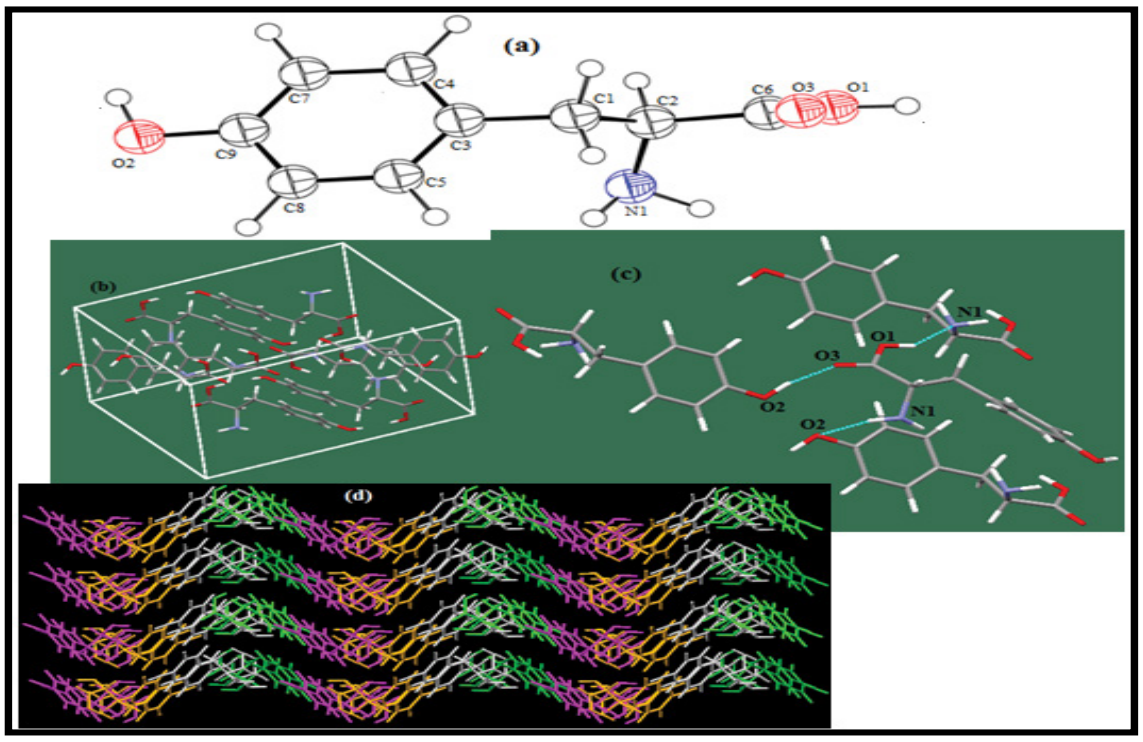

Figure 19) *Crystal structure analysis of form I of L-tyrosine- (a) Ortep diagram of asymmetric unit with 50% thermal ellipsoid probability. (b) arrangement of molecules in unit cell. (c) Hydrogen bonding patterns. (d) Molecular packing diagram (3-D network) along a-axis.*

Form I and that was found out to be the global minimum in the crystal energy landscape. The crystal structure reported in literature [27] could not be found amongst the predicted structures. The other two forms were not the lowest energy calculated structures but were found within an energy difference of approximately 2.0 kcal/mol. The lattice energy diagram is shown in Figure 22 in which the experimentally matched forms were highlighted with different colors (mentioned under legend).

Comparison of computed and experimental results:

Structures corresponding to predicted and observed polymorphs of gentisic acid and L-tyrosine found in the energy landscape, and their main characteristics are summarized in Tables 10 and 11 respectively. A fairly good proximity exists between predicted and experimental results w.r.t. lattice parameters.

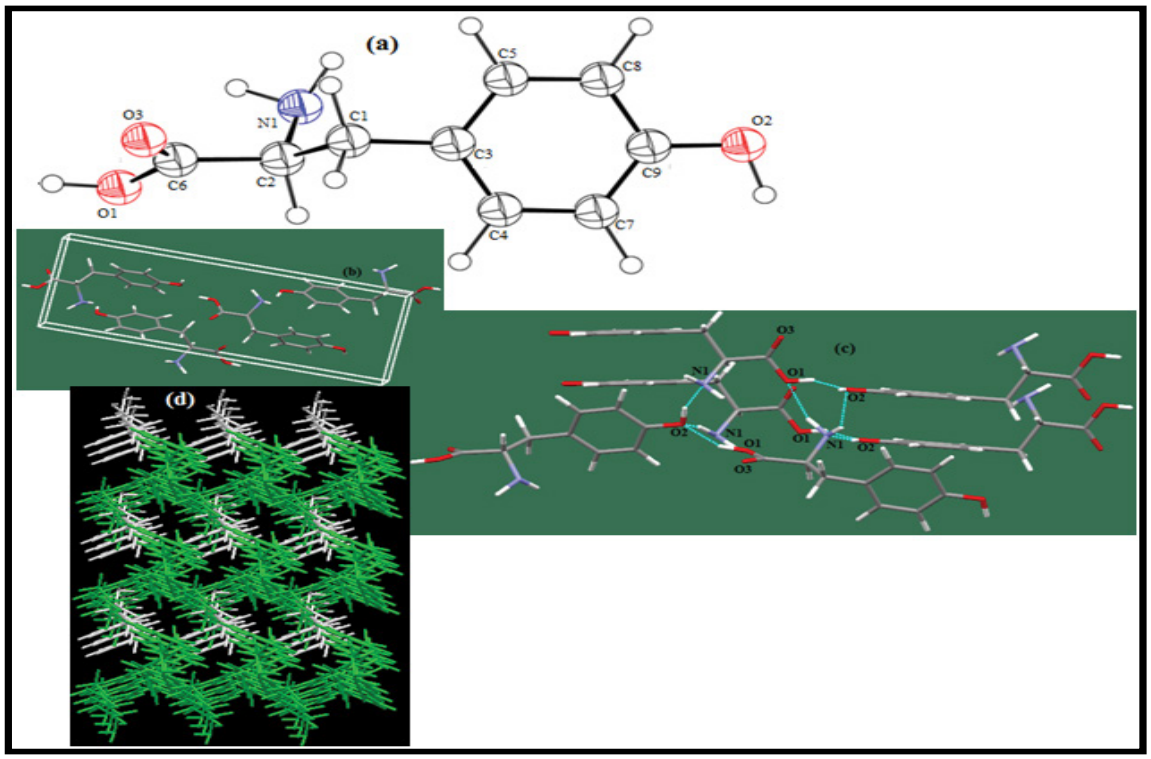

Figure 20) *Crystal structure analysis of form II of L-tyrosine- (a) Ortep diagram of asymmetric unit with 50% thermal ellipsoid probability. (b) arrangement of molecules in unit cell. (c) Hydrogen bonding patterns. (d) Molecular packing diagram (3-D network) along a-axis.*

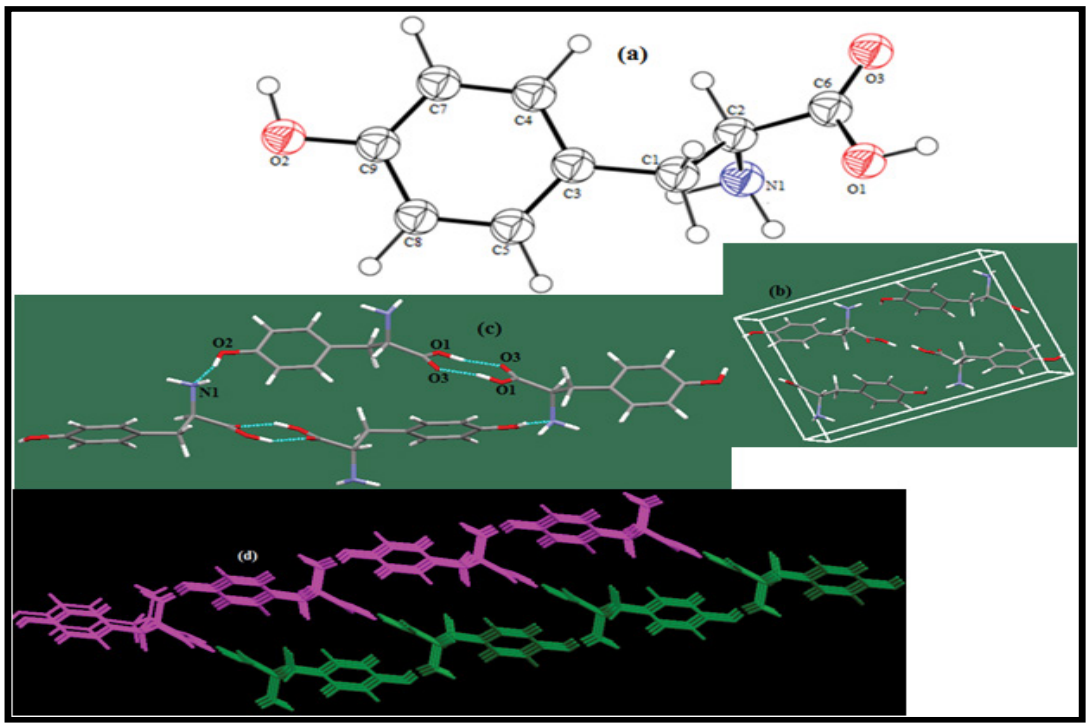

Figure 21) *Crystal structure analysis of form III of L-tyrosine-*

Crystal morphology study

Morphology of the experimentally isolated polymorphs of gentisic acid and L-tyrosine was predicted directly from their respective crystal structures. The crystal habit of observed polymorphs of these drugs was depicted by growth morphology method. Morphology of these polymorphs was evaluated assuming that the growth rate of a crystal face is proportional to its attachment energy (a habit controlling factor, defined as energy per mol of the molecule released when a new layer having thickness d_{hkl} (hkl represents the Miller indices which designate a set of faces that are equivalent by the symmetry of the crystal) is attached to the surface of the crystal). Thus the faces with the lowest attachment energies (in terms of magnitude) are the slowest growing and, thus are morphologically most important [43-46]. Now, if the attachment energy of the slowest-growing, morphologically important face is taken as a measure of the speed of growth of a crystal, it can easily explain the appearance probability of the observed forms in lattice energy landscape discussed under CSP. This further assists the lattice energy model in ranking the polymorphs based on their stability. Optical examination revealed noticeable differences in the morphology of the crystals gentisic acid and L-tyrosine which further suggests that they may be different polymorphs.

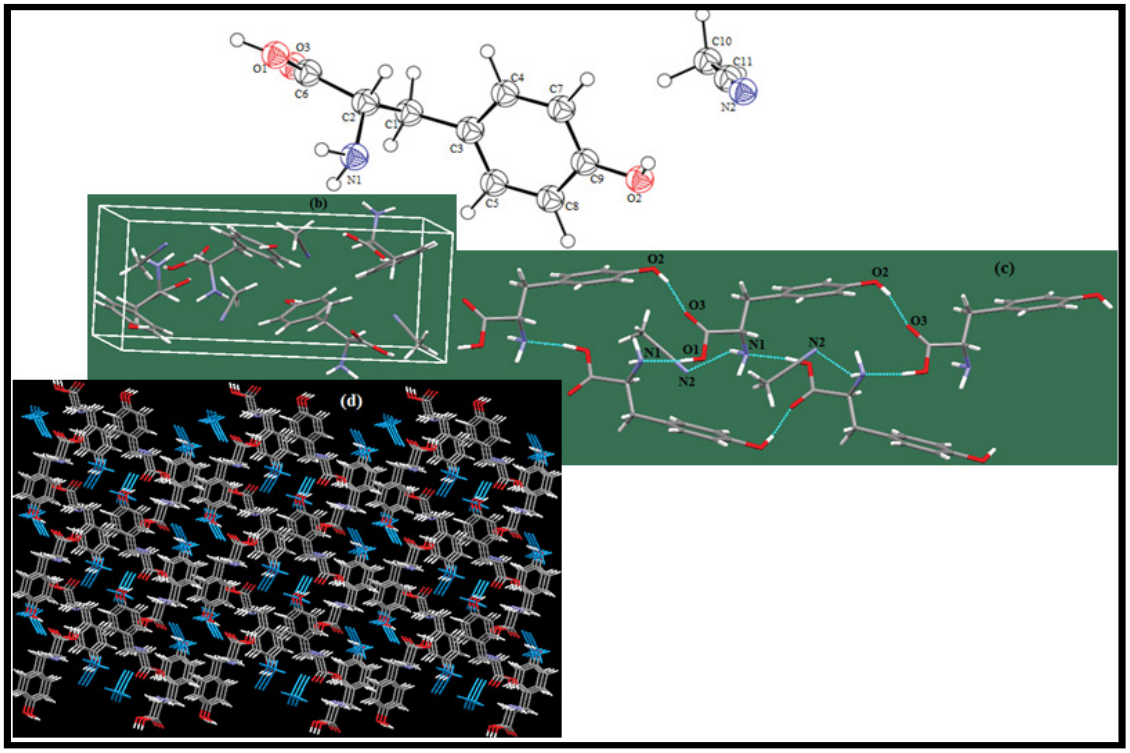

Figure 22) *Crystal structure analysis of form IV of L-tyrosine (acetonitrile solvate)- (a) Ortep diagram of asymmetric unit with 50% thermal ellipsoid probability. (b) arrangement of molecules in unit cell.(c) Hydrogen bonding patterns. (d) Molecular packing diagram (3-D network) along a-axis.*

The noteworthy difference between the simulated and the experimental morphology could be due to the absence of actual conditions provided during crystallization and also due to the influence of solvent on the growth of the experimental crystal. Crystal habit of four observed polymorphs each of gentisic acid and L-tyrosine was also predicted and the results are given in Tables 12 and 13 respectively. Figures 22-25 represent the crystal habit along with their most developed morphologically important (M.I.) faces of various polymorphs of gentisic acid and L-tyrosine respectively. The experimental morphologies of various polymorphic modifications of these drugs are shown in Figures 23-26.

Solubility of all the forms was determined in phosphate buffer 7.4 at 37◦C and is given in Tables 14 and 15 for gentisic acid and L-tyrosine respectively. The solubility study has suggested that the forms (Form IV of gentisic acid and form V of L-tyrosine) with least lattice energy are least soluble while the forms (Form III of gentisic acid and L-tyrosine) with high lattice energy are most soluble. There is approximately 2 times increase in solubility in gentisic acid in comparison with the BESKAL 02 (form present in commercial sample) and 1.62 times increase in solubility in L-tyrosine in comparison to its commercial sample (form II).

Intrinsic dissolution rate determination (IDR)

Figures 27 and 28 represent the comparative dissolution profile of various predicted and observed forms of gentisic acid and L-tyrosine respectively. Form III is found to have maximum solubility in both selected drug molecules and the percentage release was in the order: form III > form II > BESKAL 02 > BESKAL 03 > form I > form IV in case of gentisic acid and form III > form II > form I > form IV in case of L-tyrosine. This is in concordance with their lattice energy landscape data.

In vivo **studies**

The *in vivo* studies of observed forms of chosen drug molecules were performed based upon their behavioral patterns using Morris maze test and locomotor activity. Rats in the naive group in both the cases showed normal behaviour throughout the entire experimental process. The learning and memory of the rats were evaluated with the Morris water maze test. The results were interpreted as follows-

Gentisic acid

Chronic treatment with a dose of 50 mg/kg each of form II (IIb group) and form III (IIIb group) significantly ($p<0.05$) improved memory performance and shortened escape latency and increased time spent in target quadrant (TSTQ) as compared to D-galactose treated (treated control) group. However, chronic treatment with 25 mg/kg commercial gentisic acid (Ga group), form II (IIa group), form III (IIIa group) and even 50 mg/kg commercial gentisic acid (Gb group), did not show any significant ($p<0.05$) performance in memory as compared to D-galactose treated (treated control) group. Further, IIb group and IIIb group significantly ($p<0.05$) enhanced the learning and memory performance as compared to Gb group. It was also found out that there was not any significant ($p<0.05$) improvement in memory in IIIb group as compared to IIb group. The probe testing (TSTQ check) showed that retention in memory was not so significant ($p<0.05$) in Gb group as compared to control and in IIb group as compared to Gb group (Figure 29).

It was also observed (Figure 28) that none of these forms had significant effect on the memory enhancement in naïve group as the escape latencies were significantly longer and TSTQ was significantly shorter as compared with the naive (untreated) group ($P<0.05$) (Figure 28) which further showed that gentisic acid can improve learning and memory in aged rats only and has not much effect on healthy subjects (naïve group).

The D-galactose induced ageing (control group) significantly ($P<0.05$) reduced locomotor activity as compared to naïve group. Commercial gentisic acid (Gb group), form II (IIb group) and form III (IIIb group) signi cantly ($p<0.05$) improved the locomotor activity as compared to as compared to D-galactose treated (treated control) group but the three forms of gentisic acid did not differ from each other significantly ($p<0.05$) as far as the improvement in locomotor activity was concerned (Figure 28). These findings revealed that form I and II of gentisic acid has enhanced the locomotor activity in aged rats by improving their oxidative stress- induced immobilization.

L-tyrosine

Chronic treatment with a dose of 100 mg/kg each of form Ib (Ib group), form IIb (IIb group) and form IIIb (IIIb group) signi cantly ($p<0.05$) improved memory performance and shortened escape latency and increased time spent in target quadrant (TSTQ) as compared to D-galactose treated (treated control) group. However, chronic treatment with 50 mg/kg form Ia (Ia group), form IIa (form IIa group) and form III (form IIIa group) did not show any signi cant ($p<0.05$) performance in memory as compared to D-galactose treated (treated control) group. Further, IIb group and IIIb group significantly ($p<0.05$) enhanced the learning and memory performance as compared to Ib group but no significant ($p<0.05$) improvement in memory

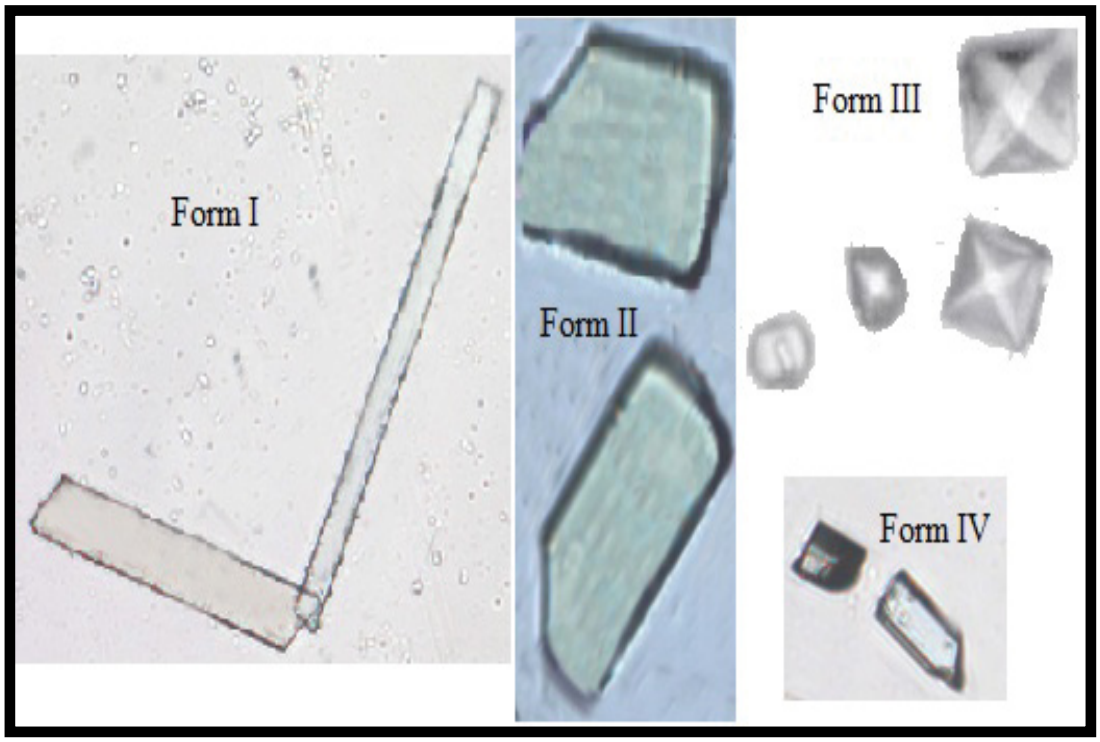

Figure 23) *Optical microscopy images showing observed morphologies of four prepared crystallites of gentisic acid (at 25 X magnification)*

TABLE 10
Crystallographic data for polymorphs of gentisic acid

Polymorph		BESKAL 02	BESKAL 03	Form I	Form II	Form III	Form IV
*Solvent used for re-crystallisation		aq EtOH+ water	aq EtOH+ $CHCl_3$ + acetone	Acetone+ ethanol	Toluene+ IPA	Methylene chloride+ ethanol	Formic acid
Crystal system		monoclinic	monoclinic	triclinic	monoclinic	monoclinic	monoclinic
Space group		P21/c	P21/c	P-1	P21/c	P21/c	P21/c
Z		4	4	2	4	4	4
a (Å)	Predt.	4.89	5.57	11.92	5.48	5.48	3.51
	Expt.	4.91	5.56	11.95	5.54	5.62	3.48
b (Å)	Predt.	11.83	4.79	9.39	4.96	4.92	11.77
	Expt.	11.83	4.87	9.41	4.91	4.90	11.80
c (Å)	Predt.	11.12	23.82	5.12	24.03	23.91	20.62
	Expt.	11.06	23.69	5.16	24	23.96	20.65
α (o)	Predt.	90	90	74.98	90	90	90
	Expt.	90	90	74.95	83.91	90	90
β (o)	Predt.	90.11	100.21	94.80	101.85	101.12	77.36
	Expt.	91.06	100.19	94.84	108.64	101.16	77.40
γ (o)	Predt.	90	90	106.80	90	90	90
	Expt.	90	90	106.76	98.69	90	90
ρ (gcm^{-3})	Predt.	1.61	1.61	1.67	1.67	1.69	1.40
	Expt.	1.60	1.62	1.66	1.65	1.70	1.60
R_{wp} (%)		5.66	5.51	7.12	7.90	5.05	5.44
E_{latt} (kcal mol^{-1})		-78.39	-77.61	-78.80	-76.68	-73.97	-113.25

*Slow evaporation method- A hot saturated solution (close to the boiling point of each of the solvent or lowest boiling solvent used from 1:1 solvent mixture) was filtered and cooled slowly at RT, Predt.- predicted parameter, Expt.- experimentally observed parameter, aq EtOH-aqueous ethanol, CHCl3- chloroform.

was found out in IIIb group as compared to IIb group. The probe testing (TSTQ check) showed that retention in memory was not so significant ($p<0.05$) in IIb group as compared to Ib group and even in IIIb group when compared with IIb group (Figure 30).

It was also observed (Figure 30) that none of these forms had significant effect on the memory enhancement in naïve group as the escape latencies were significantly longer and TSTQ was significantly shorter as compared with the naive (untreated) group ($P<0.05$) (Figure 30) which further showed that L- tyrosine can improve learning and memory in aged rats only and has not much effect on healthy subjects (naïve group).

The D-galactose induced ageing (control group) significantly ($P<0.05$) reduced locomotor activity as compared to naïve group. Form Ib (Ib group), form

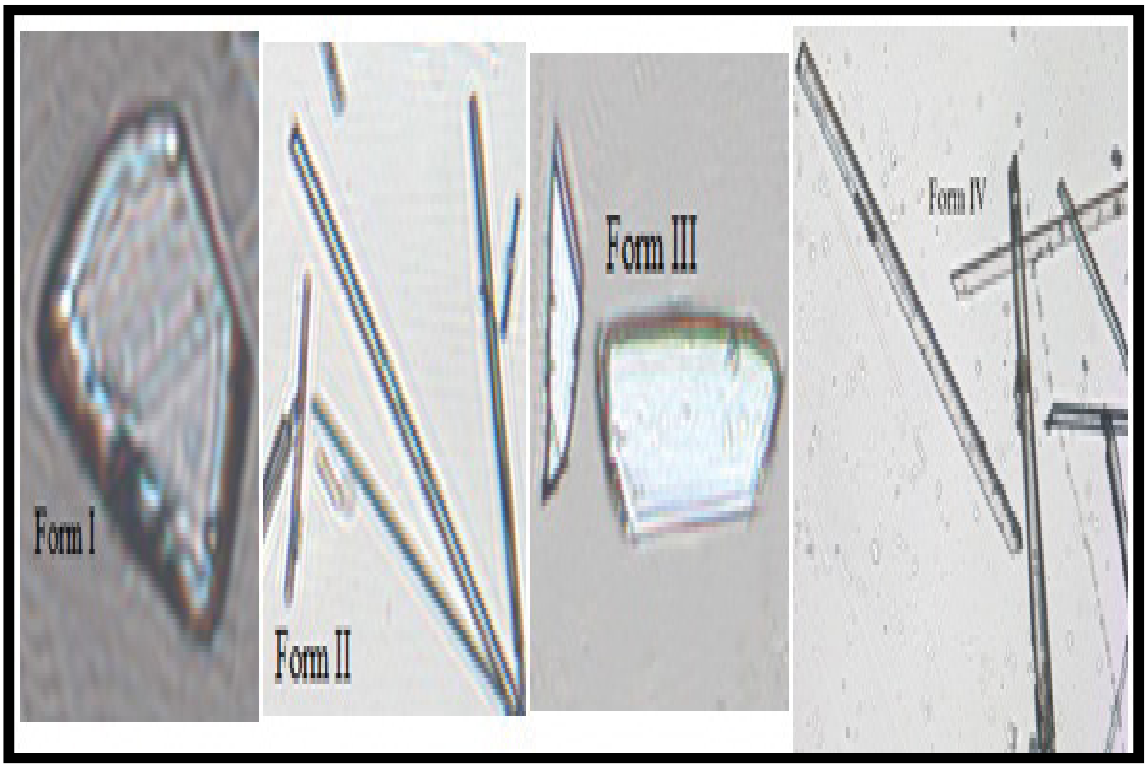

Figure 24) *Optical microscopy images showing observed morphologies of four prepared crystallites of L-tyrosine (at 25 X magnification)*

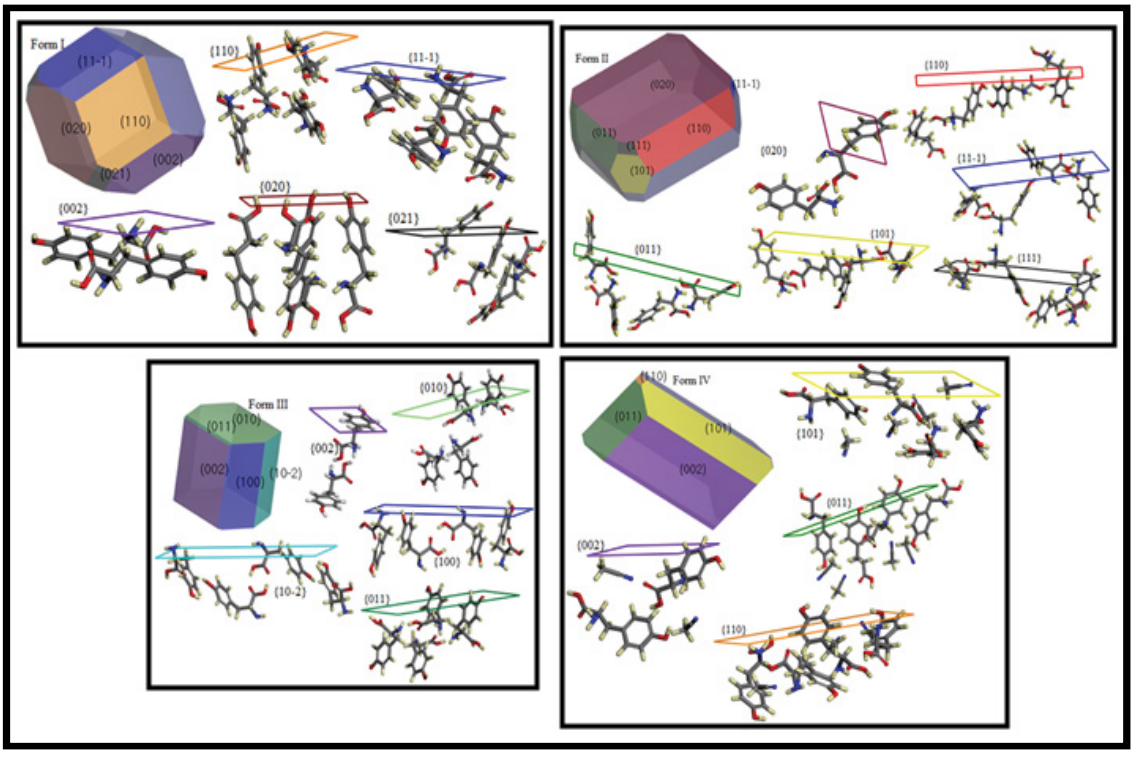

Figure 25) *Simulated crystal habit and M.I. facets of observed forms of L-tyrosine*

IIb (IIb group) and form IIIb (IIIb group) significantly (P<0.05) improved the locomotor activity as compared to as compared to D-galactose treated (treated control) group. Furthermore, IIb group and IIIb group significantly (P<0.05) improved the locomotor activity as compared to as compared to Ib group and also IIIb group significantly enhanced the locomotor activity as compared to IIb group (Figure 31). These findings revealed that form II and III of L- tyrosine has enhanced the locomotor activity in aged rats by improving their oxidative stress- induced immobilization.

DISCUSSION

The theoretical information acquired through CSP about possible polymorphs of a drug molecule is a significant step in drug development process. The lattice energy landscape would give an idea of existence of various polymorphic modifications of a drug molecule. CSP provides a wide range of information on crystal packing space featuring low energy and high density crystal structures. Biovia MS offers high- tech Polymorph Predictor module and user-friendly algorithms to predict the crystal structures of a drug substance. The variation in melting points among various forms of selected drug molecules provides an elementary idea about the different

TABLE 11

Crystallographic data for observed forms of L-tyrosine

Polymorph		Form I	Form II	Form III	Form IV (solvate)
*Solvent used for re-crystallisation		Lactic acid+ water (1:2)+ 2 drops of TFA+ antisolvent methanol	Water+ lactic acid (2:1)	Water+ lactic acid (2:1)+ antisolvent THF	Lactic acid+ water (2:1)+ 2 drops of TFA + antisolvent AcCN
Crystal system		monoclinic	orthorhombic	monoclinic	orthorhombic
Space group		C2/C	P212121	P2/c	P212121
Z		8	4	4	4
a (Å)	Predt.	9.07	7.08	5.26	6.74
	Expt.	8.99	6.91[sc] (6.97[ps])	5.83	6.81
b (Å)	Predt.	20.97	21.21	6.94	9.71
	Expt.	20.96	21.12[sc] (21.11 [ps])	6.91	9.63
c (Å)	Predt.	6.93	5.78	21.41	16.61
	Expt.	6.87	5.83 [sc] (5.90 [ps])	21.86	16.65
α (o)	Predt.	90	90	90.00	90
	Expt.	90	90	90.00	90
β (o)	Predt.	91.01	90	101.12	90
	Expt.	90.97	90	105.32	90
γ (o)	Predt.	90	90	90.00	90
	Expt.	90	90	90.00	90
ρ (g cm^{-3})	Predt.	1.53	1.42	1.69	1.40
	Expt.	1.51	1.41 (1.43)	1.57	1.35
R_{wp} (%)		5.07	7.10	10.12	6.8
E_{latt} (kcal mol^{-1})		-27.30	-26.21	-25.81	-46.45

Footnote-*slow evaporation method for form II- A hot saturated solution (close to the boiling point of each of the solvent or lowest boiling solvent used from 1:1 solvent mixture) was filtered and cooled slowly at RT, *antisolvent technique for form II, III and IV- A hot saturated solution (close to the boiling point of each of the solvent or lowest boiling solvent used from 1:1 solvent mixture) was filtered and warm methanol, THF and AcCN were added as antisolvents for form II, form III and form IV respectively, Predt.- predicted parameter, Expt.- experimentally observed parameter, THF-tetrahydrofuran AcCN- acetonitrile, sc- single crystal and ps- powder solve

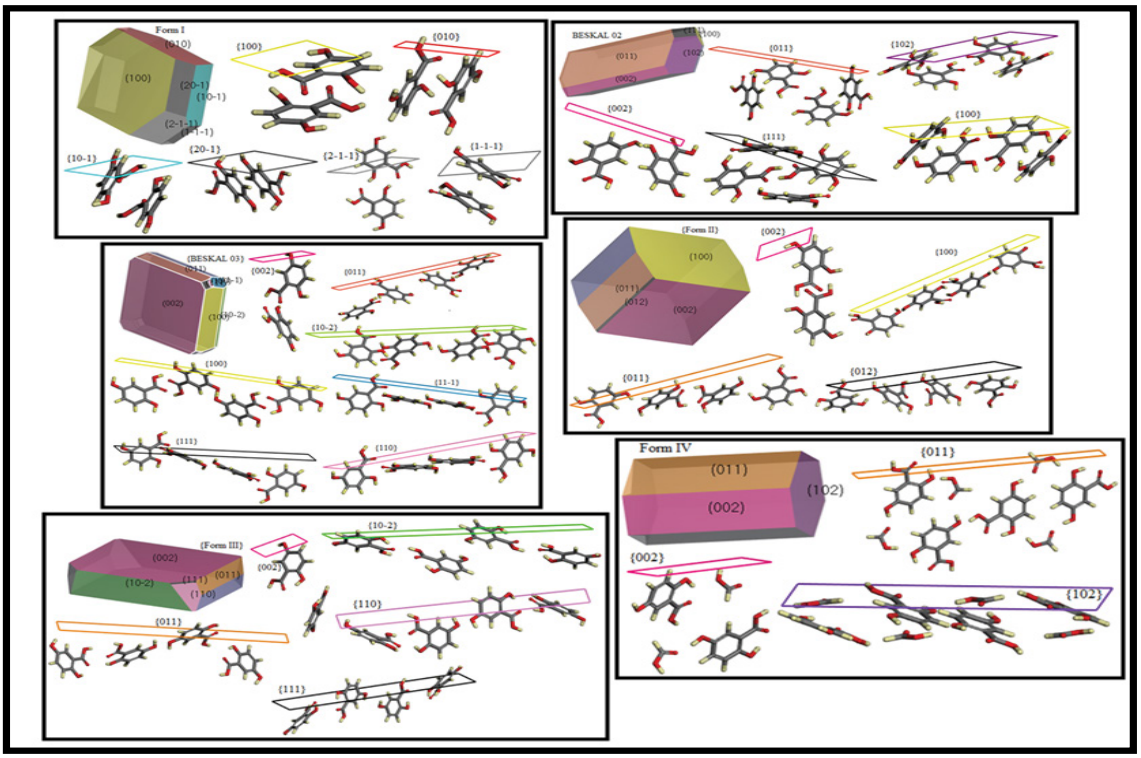

Figure 26) *Simulated crystal habit and M.I. facets of observed forms of gentisic acid*

polymorphic modifications of these moieties. Further DSC is a powerful tool to detect polymorphism in a drug molecule. The sharp endothermic peaks at different positions in observed forms indicates the presence of different solid form of drug.

TGA, a versatile technique to check the presence of solvatomorphism in drug molecules, has successfully confirmed the solvate formation in our selected drugs by showing small and broad endotherms before the melting endotherms.

The appearance of new crystal phases was confirmed by distinct differences in their PXRD patterns. Appearance of new peaks and disappearance of certain characteristic peaks justifies the formation of new solid phases.

FTIR, a quite useful spectroscopic technique to study the polymorphism/or solvatomorphism in drug molecules helps in identifying functional groups involved in hydrogen bonding. The shift in FTIR bands depicting changes in vibrational frequencies support the existence of different solid phases [52].

Crystal structure determination was done from their PXRD patterns as single

TABLE 12

Morphology prediction of various forms of gentisic acid

Polymorph	Aspect Ratio	M.I. facets	Growth Morphology		
			h k l (multiplicity)	Total % area (100 X [(total surface area of the facet)/ (total surface area)]	E_{att} (kcal/mol)
Form I	2.83	6	100 (2)	41.94	-36.63
			010 (2)	34.21	-42.28
			10-1 (2)	19.1	-70.57
			20-1 (2)	1.87	-72.42
			1-1-1 (2)	1.57	-75.54
			2-1-1 (2)	1.32	-82.72
BESKAL 02	2.70	5	011 (4)	68.17	-35.09
			102 (2)	13.65	-70.56
			002 (2)	9.82	-48.58
			111 (4)	5.49	-85.26
			100 (2)	2.87	-98.88
BESKAL 03	3.08	7	002 (2)	61.10	-18.31
			011 (4)	18.73	-53.48
			10-2 (2)	3.57	-60.24
			100 (2)	11.88	-62.17
			11-1 (4)	3.30	-73.88
			110 (4)	0.53	-75.79
			111 (4)	0.88	-76.34
Form II	3.12	4	002 (2)	43.86	-17.37
			100 (2)	25.92	-47.56
			011 (4)	18.93	-65.17
			012 (4)	10.74	-73.59
Form III	4.46	5	002 (2)	61.36	-15.61
			10-2 (2)	19.40	-24.33
			011 (4)	13.77	-30.15
			110 (4)	5.02	-39.13
			111 (4)	0.44	-74.90
Form IV	2.23	3	011 (4)	54.23	-49.33
			002 (2)	23.03	-53.03
			102 (2)	22.74	-85.66

TABLE 13

Morphology prediction of various forms of L-tyrosine

Polymorph	Aspect Ratio	M.I. facets	Growth Morphology		
			h k l (multiplicity)	Total % area (100 X [(total surface area of the facet)/ (total surface area)]	E_{att} (kcal/mol)
Form I	1.54	5	110 (4)	33.67	-82.4
			11-1 (4)	29.12	-88.13
			002 (2)	19.54	-88.23
			020 (2)	14.63	-103.50
			021 (4)	3.04	-122.13
Form II	2.41	6	020 (2)	44	-33
			110 (4)	25.91	-56.69
			011 (4)	17.80	-68.48
			101 (4)	9.20	-73.92
			11-1 (4)	1.54	-76.73
			111 (4)	1.54	-63.34
Form III	1.86	5	002 (2)	31.85	-27.52
			010 (2)	28.91	-33.71
			10-2 (2)	17.66	-34.17
			100 (2)	18.36	-34.94
			011 (4)	3.22	-39.98
Form IV	5.03	4	101 (4)	41	-55.99
			002 (2)	36.02	-41.24
			011 (4)	22.23	-98.62
			110 (4)	0.74	-108.01

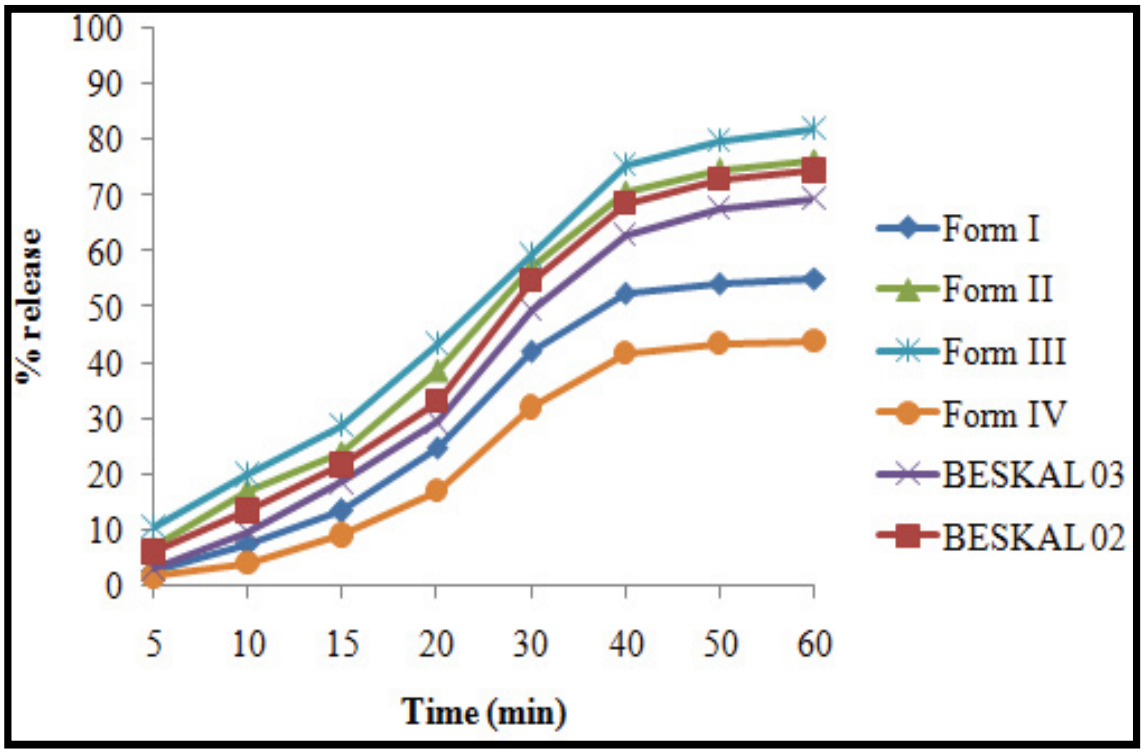

Figure 27) *Comparative in vitro release profile of observed forms of gentisic acid in phosphate buffer 7.4*

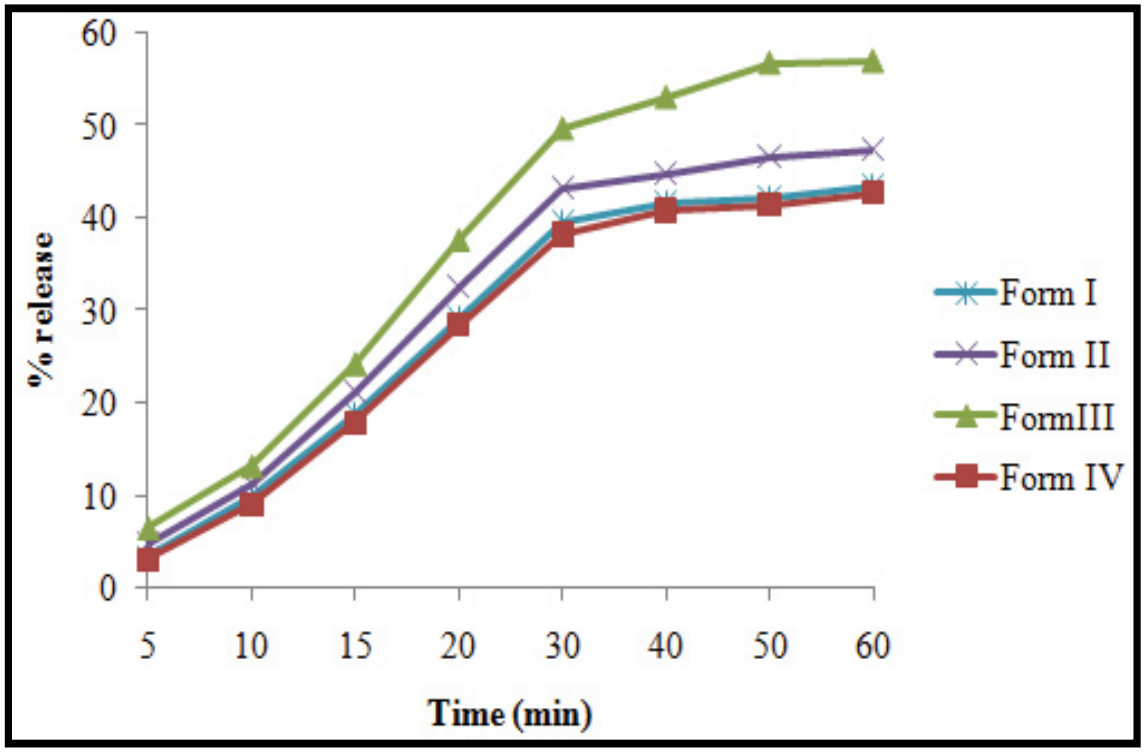

Figure 28) *Comparative in vitro release profile of observed four forms of L-tyrosine in phosphate buffer 7.4*

crystals of suitable dimensions could not be successfully obtained. Thus it is a great idea to check the fingerprints of crystals and estimate the atomic positions by exploring PXRD analysis. The crystal structures of developed forms of gentisic acid and L-tyrosine from their PXRD patterns were solved and successfully interpreted. MS software is a sophisticated tool for solving the crystal structures using extensively validated Powder Solve technology of its Reflex Plus module. The fairly good agreement between experimental and simulated PXRD patterns depicted from R_{wp} value further justifies the neatness of crystal structure determination using PXRD patterns.

The experimentally observed polymorphic forms of gentisic acid and L-tyrosine were located in the crystal energy landscape and all the forms were found as local minima within an energy difference of approximately 7.0 kcal/mol and 2.0 kcal/mol respectively.

On interpretation of predicted crystal structures of gentisic acid, it is found

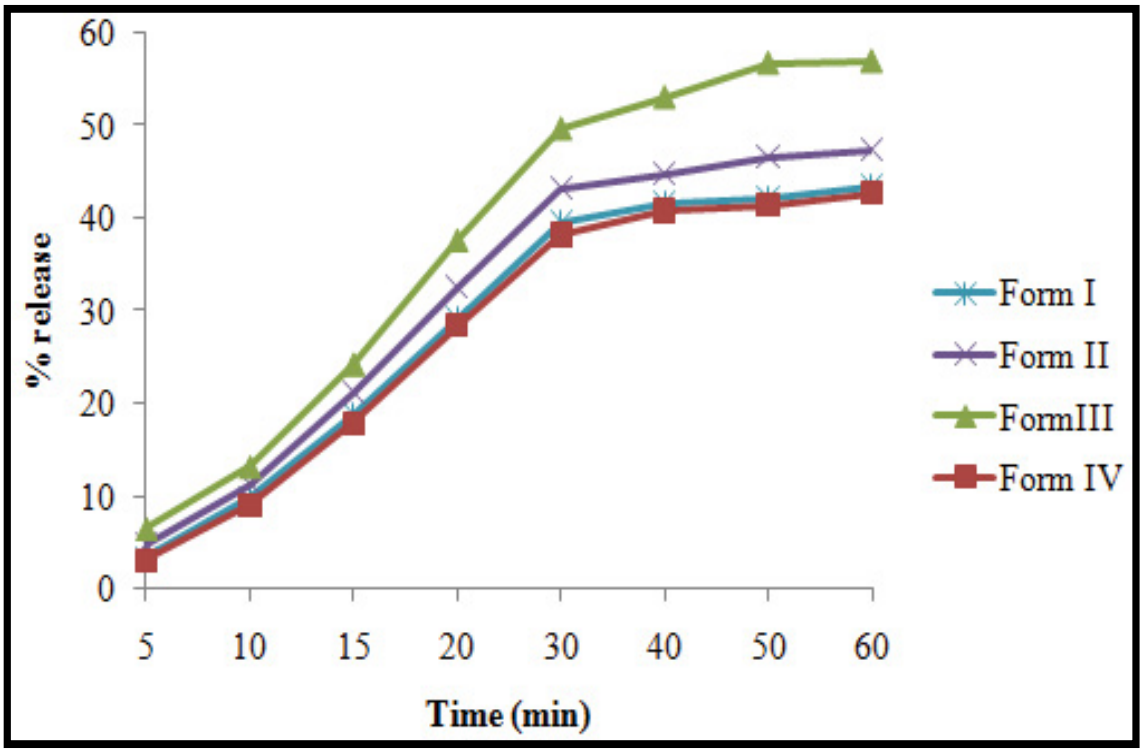

Figure 29) *Comparative in vitro release profile of observed four forms of L-tyrosine in phosphate buffer 7.4*

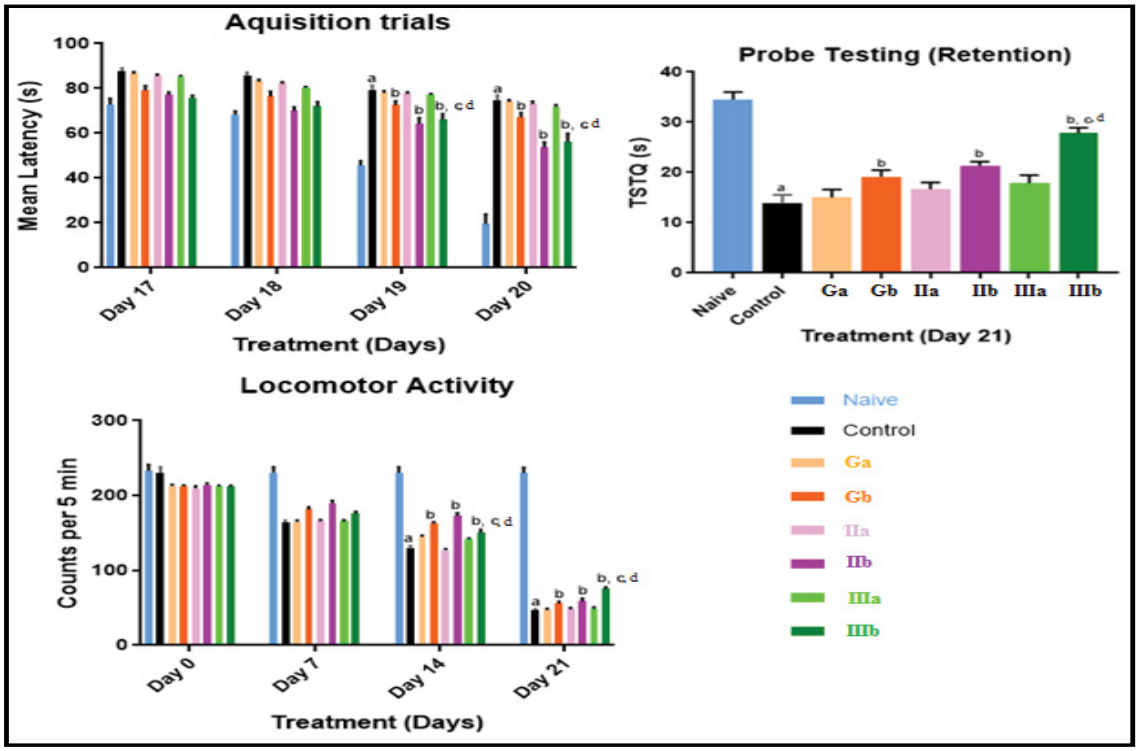

Figure 30) *Evaluation of Behavioral parameters- Effect on learning and memory checked by Morris water maze test. Data expressed as mean ± SEM ap<0.05 compared to naive group, bp<0.05 compared to control group, cp<0.05 compared to Gb group, dp<0.05 compared to IIb group, (Two way ANOVA followed by Tukey's test for evaluating acquisition trials and locomotor activity and One way ANOVA followed by Tukey's test for evaluating retention). (TSTQ- time spent in the target quadrant)*

that form I is the nearest one to the global minimum found in the lattice energy landscape. It is the 2nd predicted form in CSP run with just 0.21 kcal/mol higher energy than the global minimum and with high density value confirming it to be the most stable crystalline form. The experimentally observed form II is twentieth local minimum in the lattice energy landscape with same density value as form I [53]. Form III is the forty first local minimum with the highest density value predicted in the study. Form IV is found out to be solvatomorph of gentisic acid with formic acid (1:1). Its crystal structure was confirmed by PXRD study. The lattice energy predicted (E_{latt} = -113.25 kcalmol^{-1} and density= 1.6 gcm^{-3}) is even lesser than global minimum of gentisic acid indicating it to be most stable and crystalline form as compared to other forms of gentisic acid in the study.

On investigation of predicted crystal structures of L-tyrosine, it is clearly noticed that form I is the nearest one to the global minimum found in the

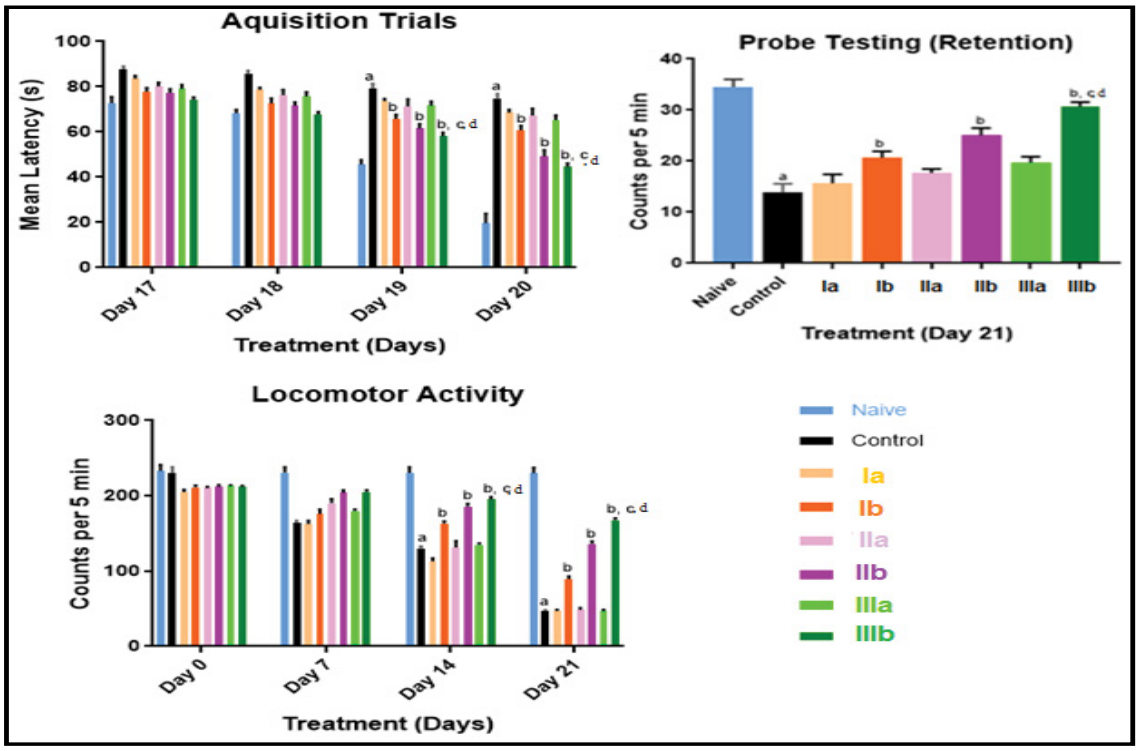

Figure 31) *Evaluation of Behavioral parameters- Effect on learning and memory checked by Morris water maze test. Data expressed as mean ± SEM ap<0.05 compared to naive group, bp<0.05 compared to control group, cp<0.05 compared to Ib group, dp<0.05 compared to IIb group, (Two way ANOVA followed by Tukey's test for evaluating acquisition trials and locomotor activity and One way ANOVA followed by Tukey's test for evaluating retention). (TSTQ- time spent in the target quadrant)*

TABLE 14

Solubility data of various forms of gentisic acid

Form	Solubility in distilled water at 37°C (mg/ml) ± SD
Form I	3.5 ± 0.7
Form II	6.3 ± 0.8
Form III	8.1 ± 1.1
Form IV	2.4 ± 0.3
BESKAL 02	5.0 ± 0.7
BESKAL 03	4.1 ± 0.5

TABLE 15

Solubility data of various forms of L-tyrosine

Form	Solubility in distilled water at 37°C (mg/ml) ± SD
Form I	0.34 ± 0.01
Form II (same as commercial sample)	0.45 ± 0.02
Form III	0.65 ± 0.02
Form V (Tyr-AcCN solvate)	0.29 ± 0.05

lattice energy landscape. It is the 2nd predicted form in CSP run with just 0.5 kcal/mol higher energy than the global minimum and with high density value confirming it to be the most stable crystalline form. The prepared form II is found out to be fifth local minimum in the lattice energy landscape. This is the same crystal form of L-tyrosine which is reported in literature [26] as confirmed by crystal structure analysis. The observed form III is the seventh local minimum predicted in the study. Form IV is the solvatomorph of L-tyrosine with acetonitrile (1:1). Its crystal structure was confirmed by PXRD study. The lattice energy predicted (E_{latt} = -46.45 kcalmol^{-1} and density = 1.35 gcm^{-3}) is even lesser than global minimum of L-tyrosine which indicated it to be most stable crystalline form as compared to other forms of L-tyrosine in the study.

The findings of morphology prediction of various polymorphic modifications of selected drugs, has well illustrated that lattice energy model has ranked the observed crystal forms in correct manner w.r.t. their stability and observing tendency.

In case of gentisic acid (Table 12), form IV is ranked first followed by I, BESKAL 02, BESKAL 03, form II and III. This is because E_{att} of M.I. facet (011) of form IV is the highest which is followed by M.I. facet (100) of form I, (011) facet of BESKAL 02, (002) facet of BESKAL 03, (002) facet of form II and (002) facet of form III . This determines the speed of growth of crystal and their observing tendency.

Table 13 clearly depicts that form I is ranked first followed by forms II and III. This is because E_{att} of M.I. facet (110) of form I is the highest which is followed by M.I. facet (101) of form IV, (020) of form II and (002) of form III. This determines the speed of growth of crystal and their observing tendency. The form IV (acetonitrile solvate or solvatomorph of L-tyrosine) has lower lattice energy value than form I which is contradictory from above statement of E_{att} criterion of ranking. This may be explained on the basis of aspect ratio. Aspect ratio (R) is one of the main characteristics of crystal habit morphologies and crystals are usually required within the range of specific values of the aspect ratio. The aspect ratio of form I is smaller than form IV [54].

It is noticed that the majority of the low energy unobserved structures have not corresponded to polymorphs because they are kinetically inaccessible, or are not minima in the free energy at experimental crystallization temperatures. The other reason for not observing these hypothetical low energy forms including the global minimum is their higher aspect ratios (>7) than the observed polymorphs. Thus some of the hypothetical structures can be eliminated based on the consideration of the predicted morphologies and growth rates, using the attachment-energy model, as they are growing as thin plates so slowly that they are unlikely to be found in competition with equally thermodynamically stable structures.

Optical microscopy, a useful analytical tool to study the crystal topography and habit aids in suggesting the appearance of different solid phases of selected drugs.

In vitro solubility study and intrinsic dissolution rate determination supports the study of polymorphism/or solvatomorphism in selected drug molecules.

All the behavioral findings including learning, memory and locomotor activity obtained from *in vivo* animal studies compliment *in vitro* dissolution study

that form II and form III of gentisic acid have markedly improved solubility as compared to commercial drug sample, making them more bioavailable. The more soluble forms II and III of L-tyrosine have apparently improved the locomotor activity as compared to commercial sample suggesting them to be useful candidates for further investigations.

CONCLUSION

The present work illustrates the significance of CSP for improving the biopharmaceutical aspects of selected antioxidants i.e. gentisic acid and L-tyrosine. The lattice energy landscape has given varied options of polymorphic forms of a drug molecule having the desired physical properties. This further could serve to focus the experimental research in their obtaining and thus lead to a more efficient experimental work, by reducing the amount of time and costs of the experimental part of the research. CSP using Polymorph Predictor module of Biovia MS has shown the tendency of gentisic acid and L-tyrosine to exist in various low energy and high density crystal forms as depicted in the crystal energy landscape. Appearance of new phase was inferred from thermal curves, PXRD scans and supported by FTIR study. Crystal structure determination from PXRD patterns proved the formation of new crystal forms of gentisic acid and L-tyrosine. The improvement in solubility and thus bioavailability is manifested in forms II and III in comparison to commercial form of gentisic acid as revealed from their *in vivo* behavioral patterns. Similarly forms II and III of L-tyrosine require more parameters to be explored in a more refined way to establish their improvement criteria in bioavailability and to prove their clinically effectiveness over commercial form. The study plays a beneficial role in accumulating the structurally diversified data to assist the anti-ageing potential of these drugs at molecular level.

REFERENCES

1. Brittain HG. The impact of polymorphism on drug development: A regulatory viewpoint. Am Pharm Rev. 2000; 3: 67- 8.
2. Grant DJ, Byrn SR. A timely re-examination of drug polymorphism in pharmaceutical development and regulation. Adv Drug Deliv Rev. 2004; 56: 237–39.
3. Haleblian J, McCrone W. Pharmaceutical applications of polymorphism. J Pharm Sci. 1969; 58: 911– 29.
4. Brittain HG. Polymorphism and solvatomorphism. J Pharm Sci. 2007; 96: 705–28.
5. Morris KR. Structural aspects of hydrates and solvates. In: Brittain HG, editor Polymorphism in pharmaceutical solids. Marcel Dekker. New York, USA. Inc.1999; 125–81.
6. Guillory JK. Generation of polymorphs hydrates solvates and amorphous solids. In: Brittain HG, editor. Polymorphism in pharmaceutical solids. New York: Marcel Dekker, Inc.1999;183– 226.
7. Doris E. Which, if any, hydrates will crystallise? Predicting hydrate formation of two dihydroxybenzoic acids. Chem Commun (Camb). 2011;47:5443-5.
8. Thayer AM. The choice of pharmaceutical crystalline form can be used to optimize drug properties, and co- crystals are emerging as new alternatives. Form and Function 2007; 85: 17- 30.
9. Sheth AR, Grant DJW. Relationship between the structure and properties of pharmaceutical Crystals. Kona. 2005;23:39-47.
10. Haber C. Anti- ageing medicine: The history: Life extension and history: The Continual Search for the Fountain of Youth. J Gerontol a Biol Sci Med Sci. 2004;59: 515–22
11. Walston J, Hadley EC, Ferrucci L, et al. Research agenda for frailty in older adults: Toward a better understanding of physiology and etiology. Summary from the American Geriatrics Society/National Institute on Aging Research Conference on Frailty in Older Adults. J Am Geriatr Soc. 2006; 54: 991–1001.
12. Bonnefoy M, Drai J, Kostka T. Antioxidants to slow ageing, facts and perspectives. Presse Med. 2002; 31: 1174-84.
13. Joshi R, Gangabhagirathi R, Venu S, et al. Antioxidant activity and free radical scavenging reactions of gentisic acid: in-vitro and pulse radiolysis studies. Free Radic Res. 2012; 46: 11-20.
14. Gülçin I. Comparison of *in vitro* antioxidant and antiradical activities of L-tyrosine and L-Dopa. Amino Acids. 2007; 32: 431-8.
15. Van Overweld, Floris WPC. Tyrosine as Important Contributor to the Antioxidant Capacity of Seminal Plasma. Chem Biol Interact. 2000.
16. Shlomo Y. Possible anti-Parkinson properties of N-(α-linolenoyl) tyrosine: A new molecule. Pharmacol Biochem Behav. 2002.
17. Pinnamaneni S, Das NG, Das SK. Formulation approaches for orally administered poorly soluble drugs. Pharmazie. 2002; 54: 291–300.
18. Bernstein J. Polymorphism in molecular crystals. Clarendon. Oxford. 2002.
19. Pikal M. Polymorphs in pharmaceutical solids. H.G. Brittain, Ed. Marcel Dekker, 1999; 398.
20. Borka L, Halebian J. Crystal polymorphism of pharmaceuticals. Acta Pharm Jugosl, 1991; 140: 71–9
21. Bernstein J. Engineering of crystalline material properties. Crystal polymorphism. 2008; 87- 109.
22. Miller JM, Collman BM, Greene LR, et al. Identifying the stable polymorphs early in the drug discovery development process. Pharm Dev.Technology .2005;10: 291- 97.
23. Haisa M, Kashino S, Hanada I, et al. The structures of 2-hydroxy-5-methylbenzoic acid and dimorphs of 2,5-dihydroxybenzoic acid. Acta Cryst. 1982;38:1480-5.
24. Adam MS, Gutmann MJ, Leech CK, et al. Stability and cooperativity of hydrogen bonds in dihydroxybenzoic acids. New J Chem. 2010; 34: 85-
25. Boggs R, Donohue J. The unit cell and space group of L-tyrosine. Acta Cryst. 1971;27: 247.
26. Mostad, A, Nissen HM, Roemming C. Crystal structure of L-tyrosine. Acta Chem Scand. 1972;26:3819-23.
27. Beyer T, Lewis T, Price SL. Which organic crystal structures are predictable by lattice energy minimisation? Cryst Eng Comm. 2001;3:178-212.
28. Price SL. From crystal structure prediction to polymorph prediction: interpreting the crystal energy landscape. Phys Chem Chem Phys. 2008;10:1996-2009.
29. Nangia A, Desiraju GR. Pseudopolymorphism: Occurrences of hydrogen bonding organic solvents in molecular crystals. Chem Commun. 1999;7:605–6.
30. Moreno Calvo E, Calvet T, Cuevas Diarte MA, et al. Relationship between the crystal structure and morphology of carboxylic acid polymorphs. Predicted and Experimental Morphologies. Cryst Growth Des 2010;10:4262-71.
31. Singh MR, Ramkrishna DA. Comprehensive approach to predicting crystal morphology distributions with population balances. Cryst Growth Des. 2013;13:1397-411.
32. Haleblian JK. Characterization of habits and crystalline modification of solids and their pharmaceutical applications. J Pharm Sci. 1975; 64:1269–88.
33. Rasenack N, Müller B. Crystal habit and tableting behavior. Int J Pharm. 2002; 244: 45– 57.
34. Myerson AS. Crystallization basics 1999 In: Myerson AS, editor. Molecular modeling applications in crystallization. New York: Cambridge University Press, USA. p: 55–105.
35. Datta S, Grant DJ. Crystal structures of drugs: advances in determination prediction and engineering. Nat Rev Drug Discov. 2004; 3: 42– 57.
36. Harris KDM, Tremayne M, Kariuki BM. Contemporary advances in the use of powder x-ray diffraction for structure determination. Angew Chem Int. 2001;40:1626.
37. Harris KDM. New opportunities for structure determination of molecular materials directly from powder diffraction data. Cryst Growth Des. 2003;3:887-95.
38. Harris KDM. Crystal structure determination from powder diffraction data. Chem Mater. 1996; 8: 2554-70.
39. Accelrys Materials Studio, V 7.0; Accelrys Inc: San Diego, CA, USA. 2013.

40. D'Hooge R, De Deyn PP. Applications of the Morris water maze in the study of learning and memory. Brain Res Brain Res Rev. 2001; 36: 60-90.

41. R.A. Young (Ed.): The Rietveld method; IUCr Monographs on Crystallography no 5; Oxford University Press; New York, USA. 1993.

42. Li J, Yuriy A, Abramov P, et al. New tricks of the trade for crystal structure refinement. ACS Central Science. 2017; 3: 726-33.

43. Fengyun CGW. Molecular Simulation and Prediction of RDX Crystal Morphology Energetic Materials. 2013; 5: 583-88.

44. Rohl AL. Computer prediction of crystal morphology. Current Opinion in Solid State and Materials Science. 2003; 7: 21–26.

45. Docherty R. Clydesdale G, Roberts KJ, et al. Application of Bravais-Friedel-Donnay-Harker, attachment energy and using models to predicting and understanding the morphology of molecular crystals. J Phys D: Appl Phys. 1991;24:89-99.

46. Prywer J. Morphological importance of crystal faces in connection with growth rates and crystallographic structure of crystal. Cryst Growth Des. 2002;2:281-6.

47. Prywer J. Effect of crystal geometry on disappearance of slow-growing faces. J Cryst Growth. 2001;224:134-44.

48. Budni J, Pacheco R, Da Silva S, et al. Oral administration of d- galactose induces cognitive impairments and oxidative damage in rats. Behav Brain Res. 2016; 302: 35-43.

49. Vorhees CV, Williams MT. Morris water maze: procedures for assessing spatial and related forms of learning and memory. Nat Protoc. 2006; 1: 848–58.

50. Nunez J. Morris water maze experiment. J Vis Exp. 2008; 19: 897.

51. Guidi M, Thomas CF. Behavioral model for assessing cognitive decline. Methods in molecular biology. 2012;829:145-53.

52. Jucker M, Oettinger R, Bättig K. Age-related changes in working and reference memory performance and locomotor activity in the Wistar rat. Behav Neural Biol. 1988;50:24-36.

53. Cohen DE, Benedict JB, Morlan B, et al. Dyeing polymorphs: The MALDI host 2,5-dihydroxybenzoic acid. Cryst Growth & Des. 2007;7:492–5.

54. David A. Towards crystal structure prediction of complex organic compounds–A report on the fifth blind test. Acta Crystallogr B. 2011; 67:535–51.